

Supplementary Materials for

Stereoselective growth of small molecule patches on nanoparticles

Jiajing Zhou¹, Matthew N. Creyer¹, Amanda Chen^{1,2}, Wonjun Yim³, René P. M. Laflleur⁴, Tengyu He³, Zhixing Lin⁴, Ming Xu¹, Pedram Abbasi¹, Jianfeng Wu⁵, Tod A. Pascal^{1,2,6}, Frank Caruso⁴, Jesse V. Jokerst^{1,3,7*}

Correspondence to: jjokerst@eng.ucsd.edu

¹Department of NanoEngineering, University of California San Diego, 9500 Gilman Drive, La Jolla, CA 92093, USA.

²UC San Diego Material Engineering Research and Education Center, University of California San Diego, 9500 Gilman Drive, La Jolla, CA 92093, USA.

³Materials Science and Engineering Program, University of California San Diego, 9500 Gilman Drive, La Jolla, CA 92093, USA.

⁴ARC Centre of Excellence in Convergent Bio-Nano Science and Technology, and the Department of Chemical Engineering, The University of Melbourne, Parkville, Victoria 3010, Australia.

⁵California Institute for Telecommunications and Information Technology, University of California San Diego, 9500 Gilman Drive, La Jolla, CA 92093, USA.

⁶Sustainable Power and Energy Center, University of California San Diego, 9500 Gilman Drive, La Jolla, CA 92093, USA.

⁷Department of Radiology, University of California San Diego, 9500 Gilman Drive, La Jolla, CA 92093, USA.

This PDF file includes:

Materials and Methods
Supplementary Text
References
Figs. S1 to S36
Tables S1 to S6
Captions for Movies S1 to S2

Other Supplementary Materials for this manuscript include the following:

Movies S1 to S2

Materials and Methods

1. Chemicals and Materials

All chemical reagents were used without further purification. bicine ($\geq 99\%$), 2-Amino-2-(hydroxymethyl)-1,3-propanediol (TRIS), phosphate buffered saline (PBS), benzene-1,4-dithiol (BDT, 99%), 4-mercaptobenzoic acid (99%), 4-aminothiophenol (97%), 4-methylbenzenethiol (MBT, 98%), 4-mercaptophenol (MCP, 97%), sodium citrate ($\geq 99\%$), sodium dodecyl sulfate (SDS, $\geq 99\%$), sodium dodecylbenzenesulfonate (SDBS, technical grade), cetyltrimethylammonium bromide (CTAB, $\geq 98.0\%$), hexadecyltrimethylammonium chloride (CTAC, $\geq 98.0\%$), silver nitrate (AgNO_3 , $\geq 99\%$), hydroquinone ($\geq 99\%$), ascorbic acid (99%), fluorescein sodium ($\geq 97.5\%$), rhodamine B ($\geq 95\%$), Azure A chloride ($\geq 70\%$), sodium borohydride (NaBH_4 , $\geq 98.0\%$), gold(III) chloride trihydrate ($\text{HAuCl}_4 \cdot 3\text{H}_2\text{O}$, $\geq 99.9\%$), hydroxylamine hydrochloride ($\text{NH}_2\text{OH} \cdot \text{HCl}$, 98%), hydrochloric acid (HCl , 36.5–38.0%), sodium hydroxide (NaOH , $\geq 98\%$), sodium chloride (NaCl , $\geq 99\%$), dimethylformamide (DMF), dimethyl sulfoxide (DMSO), were purchased from Sigma-Aldrich. Deuterium oxide (D_2O , 99.9%) and dimethyl sulfoxide- d_6 ($(\text{CD}_3)_2\text{SO}$, 99.9%) were purchased from Cambridge Isotope Laboratories. Silver nanoparticles (AgNPs) were purchased from nanoComposix, US. High-purity water with a resistivity of 18.2 M Ω cm was obtained from a Millipore water purification system.

2. General Characterization

- 2.1 Scanning electron microscopy (SEM) images were obtained using an FEI Teneo VolumeScope with an operation voltage of 10 kV.
- 2.2 Transmission electron microscopy (TEM) images were collected using a JEOL 1200 EX II TEM with an operation voltage of 80 kV.
- 2.3 High-resolution TEM images, energy-dispersive X-ray spectroscopy (EDX) profiles, and electron tomography (from -70 to +70 degrees) were acquired using a ThermoFisher Talos 200X instrument with an operation voltage of 200 kV.
- 2.4 Hydrodynamic sizes and zeta potential values were measured using a Malvern NANO-ZS90 Zetasizer.
- 2.5 Nuclear magnetic resonance (NMR) spectroscopy was conducted on a Varian Unity 300 MHz spectrometer at room temperature. Samples were dissolved in 0.6 mL $(\text{CD}_3)_2\text{SO}$ or $(\text{CD}_3)_2\text{SO}-\text{D}_2\text{O}$ two-component solvent with different volume ratios of $(\text{CD}_3)_2\text{SO}$. The samples were measured 10 min after they were dispersed in each solvent.
- 2.6 UV–visible absorption measurements were performed on an Analytik Jena SPECORD 250 PL instrument.
- 2.7 Fourier transform infrared (FTIR) spectroscopy was performed on a Bruker Tensor II FTIR spectrophotometer.

3. Synthesis of Nanoparticles

3.1 Synthesis of 20 nm Au nanoparticles (AuNPs)

AuNPs (20 nm diameter) were prepared by citrate reduction of HAuCl_4 in aqueous phase. Typically, sodium citrate (91.2 mg) in water solution (2 mL) was rapidly injected into a boiling aqueous HAuCl_4 solution (8 mg in 80 mL water) under vigorous stirring. After boiling for 15 min, the solution was cooled to room temperature.

3.2 Synthesis of 60 nm AuNPs

AuNPs of 60 nm in diameter were prepared using a seeded growth method. For the preparation, AuNPs (seeds) with a diameter of 20 nm were first synthesized. Then, the AuNPs of 20 nm in diameter were used to synthesize AuNPs of 60 nm in diameter. Briefly, 50 mL water was added into a 100 mL round-bottom flask. Then, 2 mL of the seed solution (20 nm AuNPs) and 200 μ L of 0.2 M $\text{NH}_2\text{OH}\cdot\text{HCl}$ were added to this flask consecutively. Then, 3 mL of 0.1 wt.% HAuCl_4 was added dropwise to the solution under vigorous stirring followed by reaction for 30 min at room temperature. A gradual color change from light red to dark red was observed. Finally, the concentration of sodium citrate was adjusted to 1 mM. After reacting for another 2 h, the nanoparticle dispersion was stored at 4 $^\circ\text{C}$ for further use.

3.3 Synthesis of Au nanorods (AuNRs)

AuNRs were synthesized by using seed-mediated growth method with CTAB templates.¹ The gold seeds were prepared by adding HAuCl_4 solution (5 mL, 0.5 mM) to CTAB (5 mL, 0.2 M). Then NaBH_4 (600 μ L, 10 mM) was freshly prepared and added under vigorous stirring to the mixture with an immediate color change from yellow to brownish yellow. This solution was stored at 30 $^\circ\text{C}$ for 1 h and was used as the seed solution for the synthesis of AuNRs. After that, a growth solution was prepared by adding HAuCl_4 solution (10 mL, 1 mM) to CTAB (10 mL, 0.2 M), followed by adding AgNO_3 (120 μ L, 0.1 M) and then hydroquinone (600 μ L, 0.1 M) leading to a color change from yellow to colorless. Then 300 μ L seed solution was added into the mixture. After stirring vigorously for 10 s, the mixture was stored at 30 $^\circ\text{C}$ overnight. The AuNRs solutions were centrifuged 3 times (7500 g, 15 min) to remove excess CTAB from AuNRs dispersion.

3.4 Synthesis of Au nanocubes (AuNCs)

50 nm AuNCs were synthesized using a modified three step growth process; 2-3 nm gold seeds were used to make 10 nm seeds which then served as the template for AuNCs.² To synthesize the 2-3 nm gold nanospheres, HAuCl_4 (250 μ L, 10 mM) was added to CTAB (9.75 mL, 100 mM) in a 20 mL scintillation vial that was heated (30 $^\circ\text{C}$) using a water bath. Ice-cold NaBH_4 (600 μ L, 10 mM) was injected into the solution under vortex stirring. The seeds were stirred for 5 minutes and then stored at 30 $^\circ\text{C}$ for 3 h. Next, the 10-nm gold seeds were prepared by mixing CTAC (2 mL, 200 mM), ascorbic acid (1.5 mL, 100 mM), 50 μ L of the 2-3 nm seed solution, and HAuCl_4 (2 mL, 0.5 mM), sequentially. The solution turned deep pink and was gently stirred using a magnetic stir bar and kept at 30 $^\circ\text{C}$ for 15 min. The 10 nm seeds were split into three 1.8-mL aliquots, centrifuged (2800 g, 30 min), redispersed in H_2O , and then combined to a total volume of 1 mL. The 10 nm seed solution (1 mL) was centrifuged (2800 g, 30 min) once more and redispersed in CTAC (~1 mL, 20 mM) to an optical density of 5. Lastly, the gold nanocubes were prepared by adding NaBr (150 μ L, 20 mM), 10 nm seed (25 μ L, OD = 5), ascorbic acid (1950 μ L, 10 mM) dropwise, and HAuCl_4 (30 mL, 0.5 mM) to a CTAC solution (30 mL, 100 mM) in a 100 mL round bottom flask heated to 30 $^\circ\text{C}$ under mild stirring. The reaction mixture turned from colorless to pinkish/purple over the course of 30 minutes. The final cube solution was washed two times (3000 g, 10 min) and redispersed in water each time to reach the desired optical density of 5.

4. Synthesis of Patchy Nanoparticles

4.1 Synthesis of Au-pBDT patchy nanoparticles with 60 nm AuNPs

For a typical synthesis of Au-pBDT nanoparticles, 50 μ L of 60 nm AuNPs and 100 μ L of 0.5wt% SDS were added to 2 mL bicine buffer (pH 8.5, 10 mM). After vigorous stirring for 10 min, 60 μ L BDT solution (2 mg mL^{-1} in DMF) was added to the above solution. The reaction was

stirred for 20 h. Then, the resulting patchy nanoparticles were purified by centrifugation (1600 g, 10 min) to remove the supernatant. The pellets were resuspended in water for future use.

4.2 Time-dependent synthesis of Au-pBDT patchy nanoparticles

To investigate the effect of time interval between BDT and AuNPs, we modified the protocol slightly. In brief, 60 μL BDT solution (2 mg mL^{-1} in DMF) was first added to 2 mL bicine buffer (pH 8.5, 10 mM) containing 100 μL 0.5 wt% SDS. Afterwards, 50 μL of AuNPs (60 nm) were added into the above solution at different time points (e.g., 0 min, 10 min, 30 min, 1 h, 3 h and 6 h, respectively). After reaction for 20 h, the resulting patchy nanoparticles were purified by centrifugation (1600 g, 10 min) to remove the supernatant. The pellets were resuspended in water for future use.

4.3 Temperature-dependent synthesis of Au-pBDT patchy nanoparticles

To investigate the effect of temperature on the patchy nanoparticle, we modified the protocol slightly. In a pre-heated water bath (50 $^{\circ}\text{C}$), 100 μL of 0.5 wt% SDS were added to 2 mL bicine buffer (pH 8.5, 10 mM). After gentle stirring for 5 min, 50 μL of 60 nm AuNPs were added into above solution. After another 5 min, 60 μL BDT solution (2 mg mL^{-1} in DMF) was added. The reaction was stirred for 20 h. Then, the resulting patchy nanoparticles were purified by centrifugation (1600 g, 10 min) to remove the supernatant. The pellets were resuspended in water for future use.

4.4 Synthesis of Au-pBDT patchy nanoparticles using different pH and buffer solution

To investigate the effects of pH, buffer with different pH were first prepared. The pH of the bicine buffers (10 mM) were adjusted to 8.5, 10, and 12 by varying the concentration of NaOH solution. PBS buffer (10 mM) was used for pH 7.4 medium, and pH 4 buffer were prepared by adding HCl into PBS buffer. In a typical synthesis, 100 μL of 0.5 wt% SDS were added to 1.9 mL buffer. After gentle stirring for 5 min, 50 μL of 60 nm AuNPs were added into above solution. After another 5 min, 60 μL BDT solution (2 mg mL^{-1} in DMF) was added. The reaction was stirred for 20 h. Then, the resulting patchy nanoparticles were purified by centrifugation (1600 g, 10 min) to remove the supernatant. The pellets were resuspended in water for future use.

To investigate the role of amine group in the buffer, amine-free solution (i.e., NaOH) and TRIS buffer were prepared first. Specifically, NaOH (1 M) was used to prepare the basic solution with different pH (i.e., 8.5, 10, and 12) and TRIS buffer (pH 8.5, 10 mM) was prepared. In a typical synthesis, 100 μL of 0.5 wt% SDS were added to 1.9 mL NaOH solution or TRIS buffer. After gentle stirring for 5 min, 50 μL of 60 nm AuNPs were added into above solution. After another 5 min, 60 μL BDT solution (2 mg mL^{-1} in DMF) was added. The reaction was stirred for 20 h. Then, the resulting patchy nanoparticles were purified by centrifugation (1600 g, 10 min) to remove the supernatant. The pellets were resuspended in water for future use. The pH of the solution was measured by either a pH meter or pH strips.

4.5 The stability of the Au-pBDT patchy nanoparticles

Here, stability refers to the stability of the patches on Au and/or the colloidal stability of the Au-pBDT patchy nanoparticles. To investigate the stability of patches on Au, we prepared some media or solvent including 50 mM NaCl, 1 \times PBS buffer, 0.02 M HCl, 0.02M NaOH, DMF, and DMSO. Au-pBDT Janus nanoparticles were first centrifuged and then resuspended in these media. After 1 h of incubation, the nanoparticles were collected by centrifugation (2000 g, 10 min) to remove the

supernatants. TEM was used to monitor the patch size on AuNPs after such treatment. For high temperature treatment, Au-pBDT nanoparticles were resuspended in water and heated to 90 °C via a thermal incubator. The sample was then kept at 90 °C for 3 h. The colloidal stability was evaluated by the UV-vis spectra because the LSPR peak of Au can indicate the dispersity of the Au-pBDT nanoparticles.

4.6 Synthesis of patchy nanoparticles with a second thiol-carrying molecules

To induce the surface ligand segregation on AuNPs, a second thiol-carrying molecule was added into the systems: 4-methylbenzenethiol (MBT), 4-mercaptophenol (MCP), 4-mercaptobenzoic acid (MBA), or 4-aminothiophenol (ATP). To validate if those mono-thiol molecules will form patches, 50 μL of AuNPs were added into 2.0 mL bicine buffer with 100 μL 0.5 wt% SDS. After stirring for 10 min, 60 μL of the thiol-carrying molecules were added dropwise. The concentration for each stock solution were 1.75 mg mL^{-1} (MBT) 1.74 mg mL^{-1} (MCP), 2.14 mg mL^{-1} (MBA), and 1.76 mg mL^{-1} (ATP), respectively. The products were collected by centrifugation (1600 g, 10 min) after 20 h, and measured by UV-vis spectrometer and TEM.

The binary ligand system were then employed to modulate the ligand segregation. In a typical synthesis, 50 μL of AuNPs were first added to 0.35 mL water followed by 100 μL 0.5 wt% SDS solution. After stirring for 10 min, different amounts of thiol-carrying molecules in DMF (i.e., 1.75 mg mL^{-1} (MBT), 1.74 mg mL^{-1} (MCP), 2.14 mg mL^{-1} (MBA), or 2.14 mg mL^{-1} (ATP)) were added into the above solution. After gentle stirring for 10 min, 60 μL BDT solution (2 mg mL^{-1} in DMF) was added. After another 5 min of gentle mixing, 1.5 mL bicine buffer (pH 8.5, 10 mM) was added dropwise. The reaction was stirred for 20 h. The resulting patchy AuNPs were then purified by centrifugation (1500 g, 10 min) to remove the supernatants. The pBDT-patched AuNPs were resuspended in water for future use. The volume of added thiol-carrying molecules solution was adjusted (i.e., 10 μL , 30 μL , and 60 μL) to investigate the effect of concentration of second ligand for the final patchy morphology.

4.7 Surface modification of AuNPs by using mono-thiol molecules

To investigate if mono-thiol molecules can form patches on AuNPs, we next used them alone without BDT. In a typical synthesis, 50 μL of 60 nm AuNPs and 100 μL of 0.5 wt% SDS were added to 2 mL bicine buffer (pH 8.5, 10 mM). After vigorous stirring for 10 min, 60 μL mono-thiol molecule solution was added to the above solution. The reaction was stirred for 20 h. Then, the resulting nanoparticles were purified by centrifugation (2000 g, 10 min) to remove the supernatant. The pellets were resuspended in water and used for TEM characterization. The mono-thiol molecules were dissolved in DMF, i.e., 1.75 mg mL^{-1} (MBT), 1.74 mg mL^{-1} (MCP), 2.14 mg mL^{-1} (MBA), or 2.14 mg mL^{-1} (ATP), respectively.

4.8 Synthesis of patchy nanoparticles with different aromatic dyes

An aromatic dye was added into the system to modulate the location of AuNPs in the patches. The choice of the dyes was selected based on the charge of the molecules: negatively charged dye (fluorescein sodium), zwitterionic dye (rhodamine B), and positively charged dye (Azure A chloride). In a typical synthesis, 50 μL of AuNPs were first added to 0.35 mL water followed by 100 μL 0.5 wt% SDS solution. After stirring for 10 min, different amount of dye solution (i.e., 5 mg mL^{-1} fluorescein sodium, 5 mg mL^{-1} rhodamine B, or 1 mg mL^{-1} Azure A chloride) was added into the above solution. After gentle stirring for 10 min, 60 μL BDT solution (2 mg mL^{-1} in DMF) was added to the above mixture. After another 5 min gentle mixing, 1.5 mL bicine buffer (pH 8.5,

10 mM) were added dropwise. The reaction was stirred for 20 h. The resulting patchy AuNPs were then purified by centrifugation (1500 g, 10 min) to remove the supernatants. The pBDT-patched AuNPs were resuspended in water for future use. The volume of added thiol-carrying molecules solution was adjusted to investigate the effect of concentration of dye molecules for the final patchy morphology.

4.9 Synthesis of patchy nanoparticles (60 nm AuNPs) in a ternary system

To modulate the number of patches on single AuNP, we concurrently introduced two thiol-carrying molecules (i.e., MBA and ATP) in the system because ATP can induce two patches and MBA can induce more than 5 patches on AuNPs. In a typical synthesis, 50 μL of AuNPs were first added to 0.35 mL water followed by 100 μL 0.5 wt% SDS solution. The mixture was stirred for 10 min. Meanwhile, MBA (2.14 mg mL⁻¹) and ATP (1.76 mg mL⁻¹) were mixed first to prepare the mixed ligand solution (30 μL). The mixed ligand solution was then added dropwise into the AuNP solution. After gentle stirring for 10 min, 60 μL BDT solution (2 mg mL⁻¹ in DMF) was added. After another 5 min, 1.5 mL bicine buffer (pH 8.5, 10 mM) was added dropwise. The reaction was stirred for 20 h. The resulting patchy AuNPs were then purified by centrifugation (1500 g, 10 min) to remove the supernatants. The pBDT-patched AuNPs were resuspended in water for future use. We also compared the results with patchy nanoparticles prepared from 60 μL mixed ligand solution (data not shown here), and we found that using 30 μL mixed ligand solution can produce uniform morphology and less free pBDT nanoparticles in the solution. The average number of the patches on individual nanoparticles were summarized based the TEM images of 50 nanoparticles, and the final results were calculated in triplicate batches of particles.

4.10 Synthesis of Au-pBDT patchy nanoparticles with 20 nm AuNPs

50 μL of AuNPs (20 nm) stabilized by SDS were first added to 2 mL bicine buffer (pH 8.5, 10 mM). After vigorous stirring for 10 min, 60 μL BDT solution (2 mg mL⁻¹ in DMF) was added to the above solution. The reaction was stirred for 20 h. The resulting patchy nanoparticles were then purified by centrifugation (8000 g, 10 min) to remove the supernatants. The pellets were resuspended in water for future use. The size of the patches can be tuned by varying the concentration of BDT or AuNPs in the final reaction solution.

To tune the number of the patches on 20 nm AuNPs, thiol-carrying molecules in DMF solution (i.e., 2.14 mg mL⁻¹ MBA or 2.14 mg mL⁻¹ ATP) were added before adding BDT. After gentle stirring for 10 min, 60 μL BDT solution (2 mg mL⁻¹ in DMF) was added to the above mixture. The volume of added thiol-carrying molecules solution was fixed at 10 μL (molar ratio of BDT to thiol additive = 6:1).

4.11 Synthesis of pBDT-patched AuNRs

The addition of BDT into as-prepared AuNR induces aggregation of AuNRs. Therefore, the excess CTAB in the AuNR stored solution were first removed by ligand exchange. Specifically, 1 mL of AuNR-CTAB were added into 10 mL 0.5% SDS solution with vigorous stirring. After sonication for 1 min, the solution kept stirring overnight. AuNR-SDS was obtained by centrifugation (8000 g, 10 min) to remove the supernatants. The AuNR pellets were resuspended in water for future use.

In a typical synthesis of pBDT-patched AuNRs, 100 μL of AuNRs were first added to 2 mL bicine buffer (pH 8.5, 10 mM) followed by 100 μL 0.5 wt% SDS solution. After stirring for 10 min, 60 μL BDT solution (2 mg mL⁻¹ in DMF) was added to the above solution. The reaction was

stirred for 20 h. The resulting patchy AuNRs were then purified by centrifugation (8000 g, 10 min) to remove the supernatants. The pBDT-patched AuNRs were resuspended in water for future use. The size of the patches can be tuned by varying the concentration of BDT in the final reaction solution.

To tune the number of the patches on AuNRs, 2.14 mg mL⁻¹ MBA were added before adding BDT. The volume of added thiol-carrying molecules solution was fixed at 10 μL (molar ratio of BDT to thiol additive = 6:1).

4.12 Synthesis of pBDT-patched AuNCs

The excess CTAB in AuNC was first removed via three rounds of centrifugation (2000 g, 10 min). In a typical synthesis of pBDT-patched AuNCs, 100 μL of AuNCs were first added to 2 mL bicine buffer (pH 8.5, 10 mM), followed by 100 μL 0.5 wt% SDS solution. After stirring for 10 min, 60 μL BDT solution (2 mg mL⁻¹ in DMF) was added to the above solution. The reaction was stirred for 20 h. The resulting patchy AuNCs were then purified by centrifugation (2000 g, 10 min) to remove the supernatants. The pBDT-patched AuNCs were resuspended in water for future use. The size of the patches can be tuned by varying the concentration of BDT in the final reaction solution.

To tune the number of the patches on AuNCs, thiol-carrying molecules in DMF solution (i.e. 2.14 mg mL⁻¹ MBA or 2.14 mg mL⁻¹ ATP) were added before adding BDT. After gentle stirring for 10 min, 60 μL BDT solution (2 mg mL⁻¹ in DMF) was added to the above mixture. The volume of added thiol-carrying molecules solution was fixed at 10 μL (molar ratio of BDT to thiol additive = 6:1).

4.13 Synthesis of pBDT-patched AgNPs

200 μL of AgNPs (55 nm) stabilized by sodium citrate were first added to 2 mL bicine buffer (pH 8.5, 10 mM) containing 100 μL of 0.5 wt% SDS. After vigorous stirring for 10 min, 60 μL BDT solution (2 mg mL⁻¹ in DMF) was added to the above solution. The reaction was stirred for 3 h. The resulting patchy nanoparticles were then purified by centrifugation (2000 g, 10 min) to remove the supernatants. The pellets were resuspended in water for future use.

4.14 Assembly of patchy Au-pBDT nanoparticles into trimers

In a typical assembly process, Au-pBDT nanoparticles (OD = 2) were first dispersed in 2 mL water with gentle stirring; 50 mM NaCl was then added by dropwise. After the solution turned slightly purple, the reaction were quenched by adding 4 mL water and purified by centrifugation (800 g, 10 min). The pellets were resuspended in water and casted on TEM grids for characterization.

5. Simulation Model Constructions

5.1 Finite difference time domain simulations

Electromagnetic wave calculations were performed using Lumerical FDTD solutions software. Three dimensional simulations were performed with a background refractive index of 1.33 for H₂O, Palik complex refractive indices for gold, and a refractive index of 1.59 for BDT. An X minimum symmetric boundary condition was applied along the propagation axis of the incident electromagnetic wave (z-axis) to reduce computational cost. Absorbance and scattering measurements were taken by placing a power monitor inside and outside of the EM source, respectively. Extinction spectra were calculated upon addition of the absorbance and scattering

cross sections ($\sigma_{\text{ext.}} = \sigma_{\text{abs.}} + \sigma_{\text{sca.}}$) and subsequent normalization to the source intensity. Electric field distributions were captured using a 0.5 nm mesh size and by placing a 2D field profile monitor in the x-z plane.

5.2 MD simulation

5.2.1 Binding energies between molecules and Au via DFT calculations

First-principles DFT calculations of the binding energy of BDT, BDT (-q), BDT (-2q), Fluo, and AAC molecules on gold were performed using norm-conserving pseudopotentials in the Siesta 3.1 electronic structure package^{3,4} with a double-zeta polarized (DZP) and a mesh cutoff value of 300 Ry. To limit the range of the basis pseudoatomic orbitals, an energy shift of 0.0025 Ry was applied along with a split norm of 0.53 for the second zeta. For geometry optimizations the conjugate-gradient approach was used with a threshold of 0.04 eV Å⁻¹. For Hamiltonian solutions, and a standard diagonalization method was utilized with effective electron temperature of 0.005 eV.

The interaction of molecules with the gold surface was modeled using a (001) gold slab with 6×3×2 unit cells (128 atoms) for the dyes and 4×3×2 unit cells (96 atoms) for the BDT molecules. To avoid spurious overlap of electronic charges from neighboring cells, we used a cell size of 50 Å along the Z direction. For the integrals in the Brillouin zone in the periodic XY direction a 4×4 Monkhorst-Pack grid was used while the periodicity along Z axis was modeled with a single k-point. All atoms were allowed to relax at constant cell volume during the geometry optimization and a slab dipole correction was applied to account for asymmetric dipoles due to presence of adsorbates on one side of the gold slab.

5.2.2 Quantum chemistry calculations

Ab-initio quantum mechanics calculations were performed at the MP2/6-311G* level of theory via the Q-Chem 5.0 package.⁵ The atom-charges of pBDT₂, pBDT₄, Fluo, and AAC molecules were obtained from Ground-State Mulliken Net Atomic Charge Analysis.

5.2.3 Classical molecular dynamics simulations

All of our MD simulations were performed using the LAMMPS simulation engine.⁶ The water molecules were described by the TIP3P water model⁷ while the Na⁺ and Cl⁻ ions were described using the optimized parameters of Joung and Cheatham⁸ as detailed in **table S4**. The BDT, AAC, Fluo molecules were described using either the DREIDING force field,⁹ or the work of Heinz. *et al.*,¹⁰ as detailed in **table S5**.

We initiated each simulation in a 73×73×100 Å³ box in a slab geometry (i.e., finite in the z direction). We modelled the Au nanoparticles as a xy periodic slab based on the (001) surface of Au fcc structure (lattice constant of 4.065 Å). This slab was taken as a rigid body during the entire simulation. During our model construction, we added enough Na⁺/Cl⁻ ions to achieve overall charge neutrality.

Each MD simulation was initiated with 500 steps of conjugated gradient (CG) minimization, followed by a slow heating of the system from 0 – 323K in the canonical (constant temperature, volume and number of particles – NVT) ensemble. We used a simulation integration timestep of 1 fs. We employed a Nose-Hoover thermostat with a time relaxation constant of 100 steps. We employed the SHAKE¹¹ algorithm to constrain all bonds involving hydrogen and the H-O-H angle of the water molecules. This equilibration procedure was followed by at least 12 ns of NVT dynamics saving the trajectory (atomic x, y, and z positions and velocities) every 100 ps. Snapshots

of the systems after 0, 6, and 12 ns are presented in **figs. S26** and **S28**. The mass density-profiles in z-coordinate were calculated from the last 6 ns of our simulation and shown in **figs. S27** and **S29**.

5.2.4 Solvation free energies of molecules

Multi-stage free energy perturbation calculations were used to calculate the solvation free energy in each of BDT/Fluo/AAC. Here, we write the potential energy of the system as:

$$U(\lambda) = U_{bg} + U_1(\lambda) + U_0(\lambda) \quad (1)$$

where U_{bg} in equation 1 is a background term corresponding to interaction sites whose parameters remain constant, U_0 is a reference term corresponding to the initial interactions of the atoms that will undergo perturbation, U_1 is a term corresponding to the final interactions of these atoms, and λ is a coupling parameter varying from 1 to 0 and thus connecting the fully interacting system to one where the molecule does not interact with the solvent/mixture. The potential in eq. 1 was implemented using standard λ -dependent soft-core Lennard-Jones potentials as implemented in LAMMPS with $n = 1$ and $\alpha LJ = 0.5$. We calculated the solvation free energy via stepwise alchemical transformations during a simulation run:

$$\Delta_0^1 A = \sum_{i=0}^{n-1} \Delta_{\lambda_i}^{\lambda_{i+1}} A = -kT \sum_{i=0}^{n-1} \ln \left\langle \exp \left(-\frac{U(\lambda_{i+1}) - U(\lambda_i)}{kT} \right) \right\rangle_{\lambda_i} \quad (2)$$

where the brackets in equation 2 indicate an ensemble average. We slowly varied λ in steps of 0.05 (22 steps in total including the initial and final stages). For each stage, we performed 500 ps of NpT dynamics at 323 K and 1 bar to equilibrate the system followed by 1 ns of NpT dynamics for collecting statistics. We estimated the error in our calculated free energies at each stage by splitting the 1 ns production MD run into four sets of 250-ps runs and calculated the statistical average and variance (standard deviation). The total variance was taken as the average of the variance at each stage.

References

1. Nikoobakht, B.; El-Sayed, M. A., Preparation and growth mechanism of gold nanorods (NRs) using seed-mediated growth method. *Chem. Mater.* 2003, 15 (10), 1957–1962.
2. Park, J. E.; Lee, Y.; Nam, J. M., Precisely shaped, uniformly formed gold nanocubes with ultrahigh reproducibility in single-particle scattering and surface-enhanced Raman scattering. *Nano Lett.* 2018, 18 (11), 6475–6482.
3. Soler, J. M.; Artacho, E.; Gale, J. D.; Garcia, A.; Junquera, J.; Ordejon, P.; Sanchez-Portal, D., The SIESTA method for ab initio order-N materials simulation. *J. Phys-Condens: Mat.* 2002, 14 (11), 2745–2779.
4. Garcia, A. et al, Siesta: Recent developments and applications. *J. Chem. Phys.* 2020, 152 (20), 204108.
5. Shao, Y. et al, Advances in molecular quantum chemistry contained in the Q-Chem 4 program package. *Mol. Phys.* 2015, 113 (2), 184–215.
6. Plimpton, S., Fast parallel algorithms for short-range molecular-dynamics. *J. Comput. Phys.* 1995, 117 (1), 1–19.
7. Jorgensen, W. L.; Chandrasekhar, J.; Madura, J. D.; Impey, R. W.; Klein, M. L., Comparison of simple potential functions for simulating liquid water. *J. Chem. Phys.* 1983, 79 (2), 926–935.

8. Joung, I. S.; Cheatham, T. E., Determination of alkali and halide monovalent ion parameters for use in explicitly solvated biomolecular simulations. *J. Phys. Chem. B* 2008, 112 (30), 9020–9041.
9. Mayo, S. L.; Olafson, B. D.; Goddard, W. A., DREIDING: A generic force-field for molecular simulations. *J. Phys. Chem.* 1990, 94 (26), 8897–8909.
10. Heinz, H.; Vaia, R. A.; Farmer, B. L.; Naik, R. R., Accurate simulation of surfaces and interfaces of face-centered cubic metals using 12-6 and 9-6 Lennard-Jones potentials. *J. Phys. Chem. C* 2008, 112 (44), 17281–17290.
11. Ryckaert, J. P.; Ciccotti, G.; Berendsen, H. J. C., Numerical-integration of Cartesian equations of motion of a system with constraints - molecular-dynamics of N-alkanes. *J. Comput. Phys.* 1977, 23 (3), 327–341.

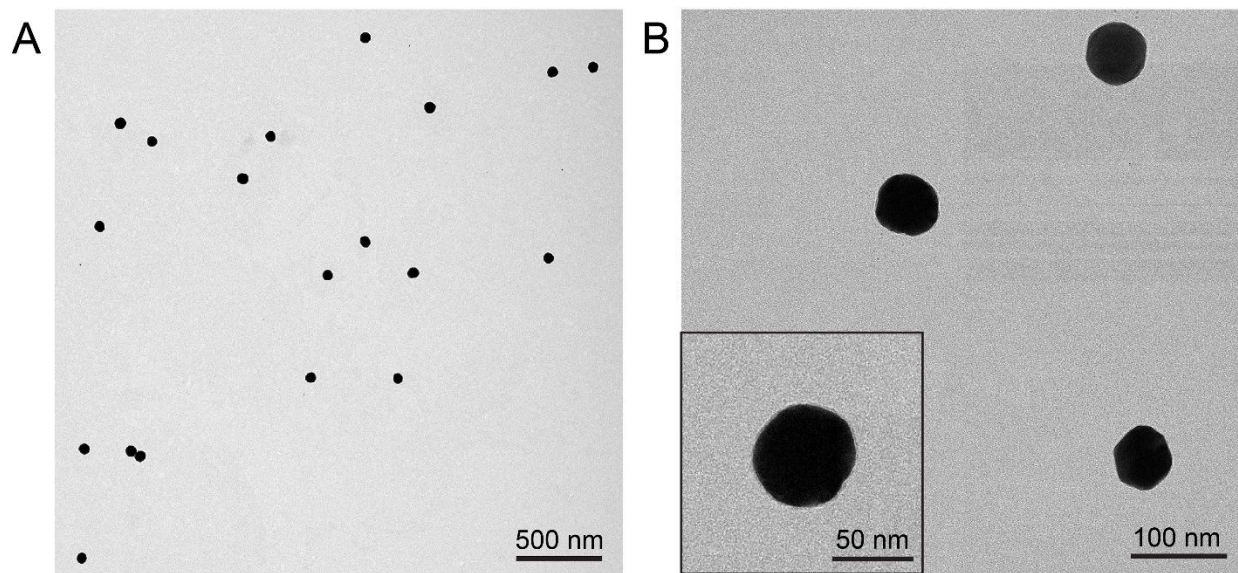


Fig. S1.

TEM images of 60 nm AuNPs used in this work. (A) Low magnification image of the AuNPs. (B) High magnification image of the AuNPs. Inset is the close-up image of one representative AuNP. The clear boundary of AuNPs indicated there was no obvious ligand shell due to the small molecule nature of the surface ligand (e.g., sodium citrate or SDS).

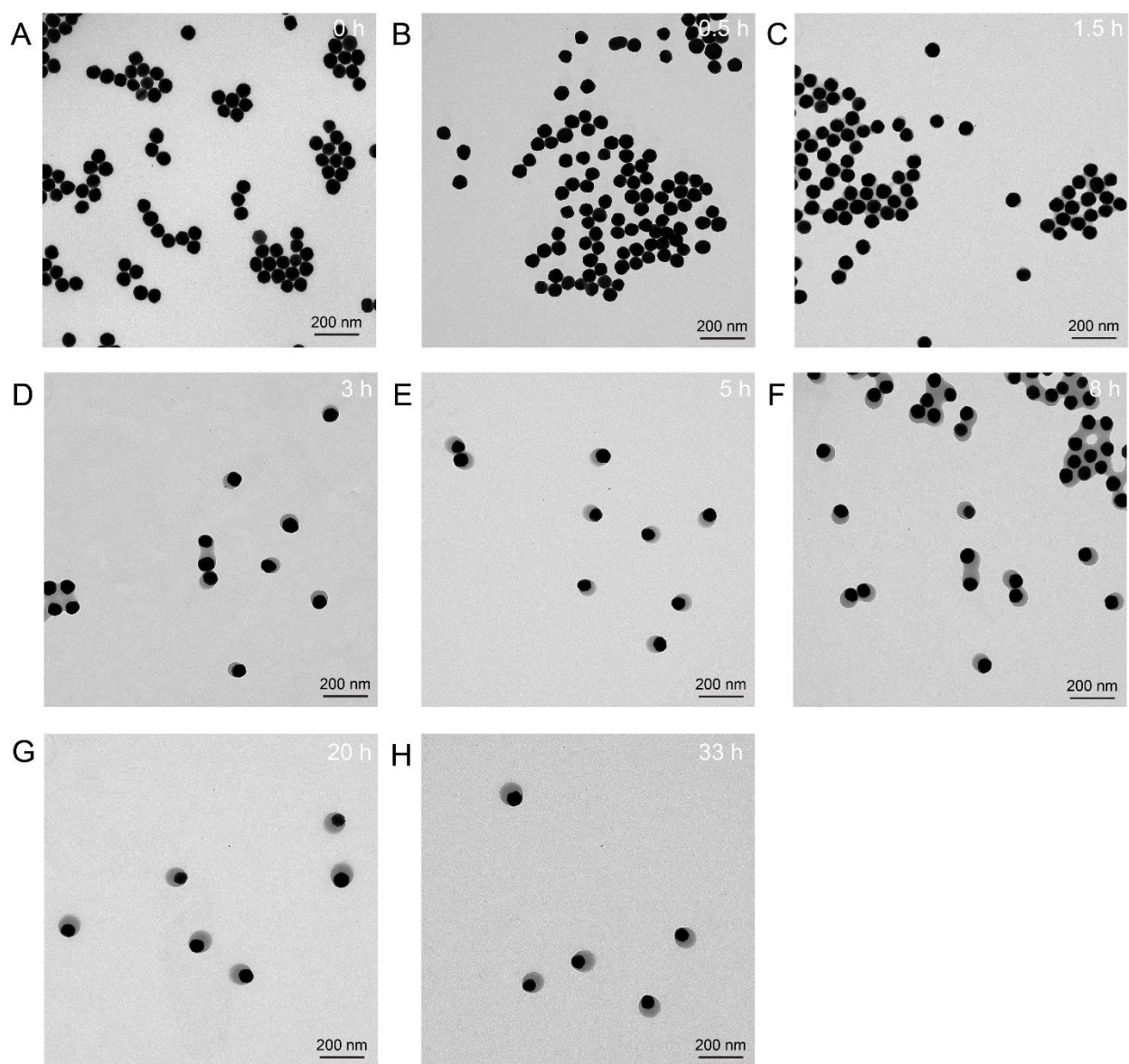


Fig. S2.

TEM images of the growth of Au-pBDT nanoparticles at different time points: (A) 0 h, (B) 0.5 h, (C) 1.5 h, (D) 3 h, (E) 5 h, (F) 8 h, (G) 20 h, and (H) 33 h. To obtain the samples at different time point, an aliquot of reaction solution (100 μ L) was taken from the reaction and the assembly was quenched by adding 20-fold excess of water. After centrifugation (1800 g, 10 min), the pellets were imaged. The results suggest that patches gradually grow larger on the surface of AuNPs, indicative of an unusual “grafting-from” strategy.

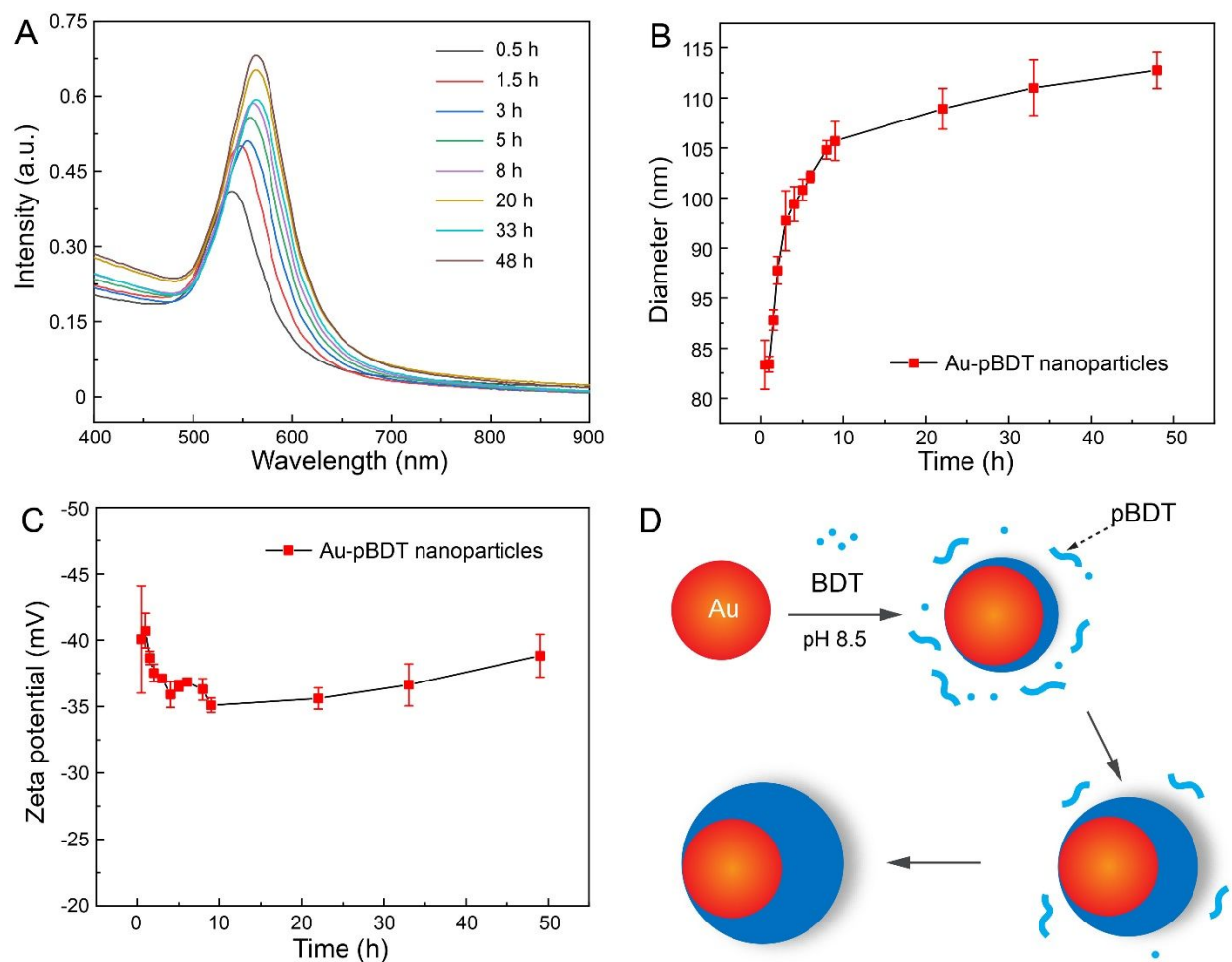


Fig. S3.

Time-dependent growth of Au-pBDT nanoparticles. (A) UV-vis extinction spectra of the Janus Au-pBDT patchy nanoparticles collected at different time points. (B) DLS result of the Au-pBDT patchy nanoparticles collected at different time points: 0.5 h, 1.0 h, 1.5 h, 2 h, 3 h, 4 h, 5 h, 6 h, 8 h, 20 h, 33 h, and 48 h. (C) Zeta potential values of Au-pBDT patchy nanoparticles (in water) at different time points in water: 0.5 h, 1.0 h, 1.5 h, 2 h, 3 h, 4 h, 5 h, 6 h, 8 h, 20 h, 33 h, and 48 h. (D) Proposed mechanisms for the bottom-up approach which combines both covalent bond and supramolecular interactions. The results suggest that the growth of Au-pBDT nanoparticles reaches equilibrium after 20 h exhibiting a high negative charge on surface. We suggest that BDT can bind to metal surface via thiol-mediated chemistry and self-polymerize into polymerized BDT (pBDT) via disulfide bonds at the beginning of the process. Later, the monomers (i.e., BDT and pBDT) can continuously assemble onto the surface of AuNPs via π - π interactions allowing for the bottom-up formation of 3D patches.

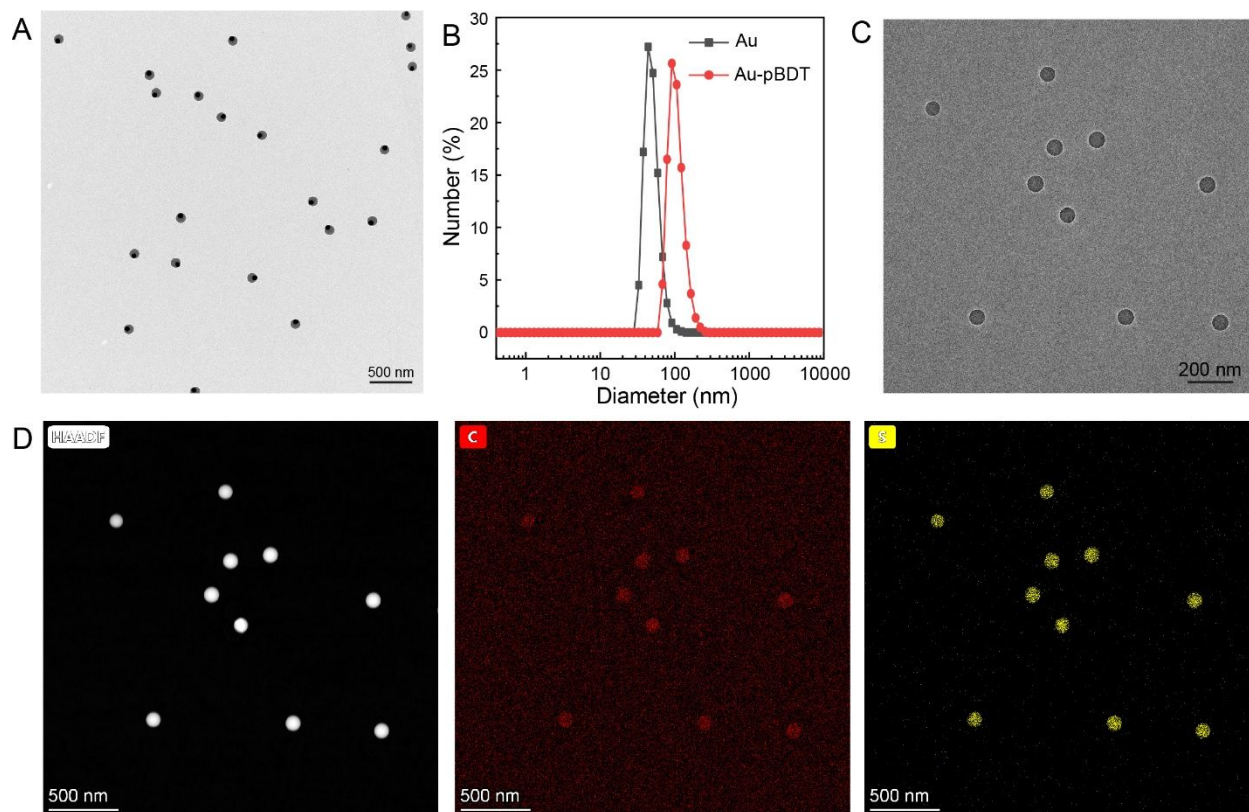


Fig. S4.

(A) TEM image of Au-pBDT patchy nanoparticles at low magnification. (B) DLS result of the Au-pBDT patchy nanoparticles. The clear background in TEM image indicated negligible free pBDT nanoparticles in the sample. The low polydispersity index before (PDI, 0.089) and after (PDI, 0.049) pBDT coating suggests monodispersity. (C) TEM image of pBDT polymeric nanoparticles. These products were obtained by the same protocol without adding AuNPs in the reaction solution. (D) EDX elemental mapping of pBDT nanoparticles.

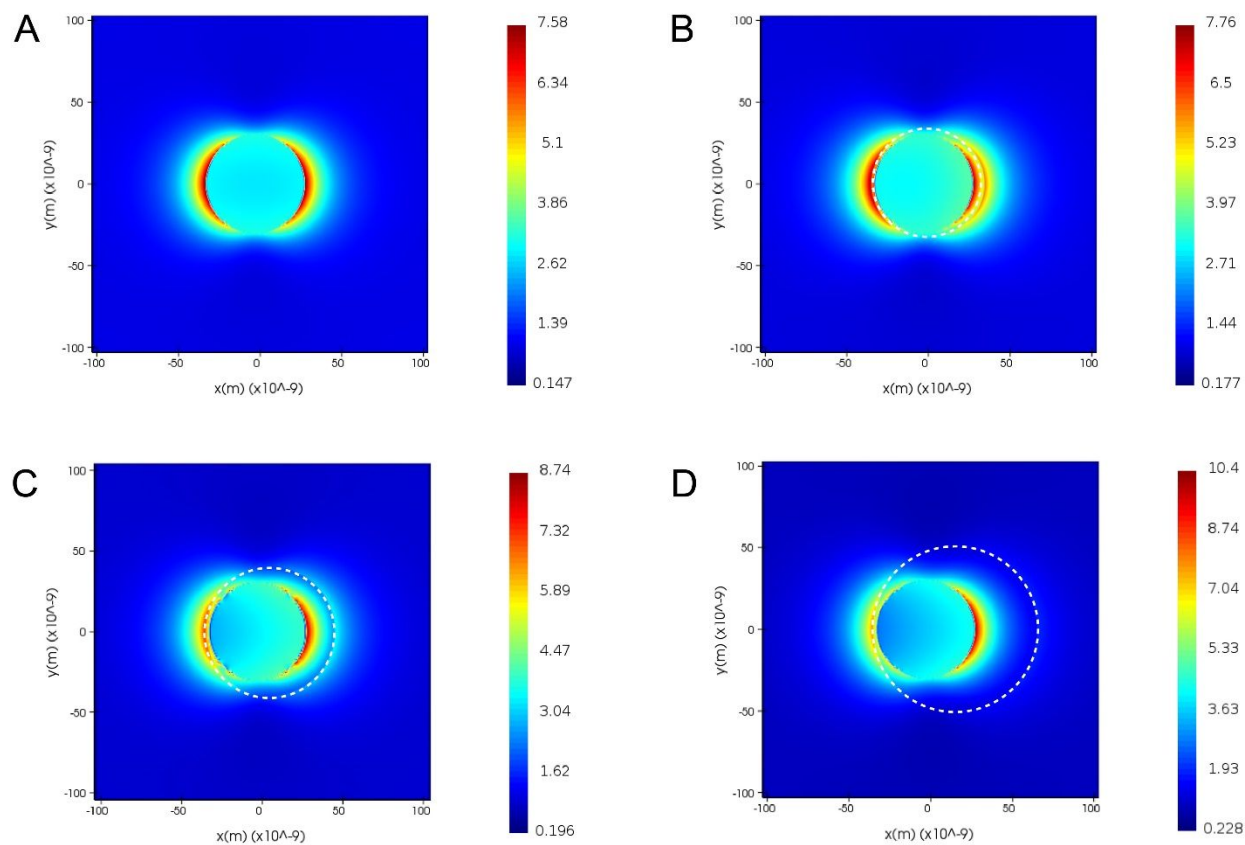


Fig. S5.

Simulated electric field intensity enhancement contours of the Janus Au-pBDT patchy nanoparticles with different size of patch: 0 nm (A), 2 nm (B), 20 nm (C), and 40 nm (D). The white dash circles indicate the area of the pBDT patches.

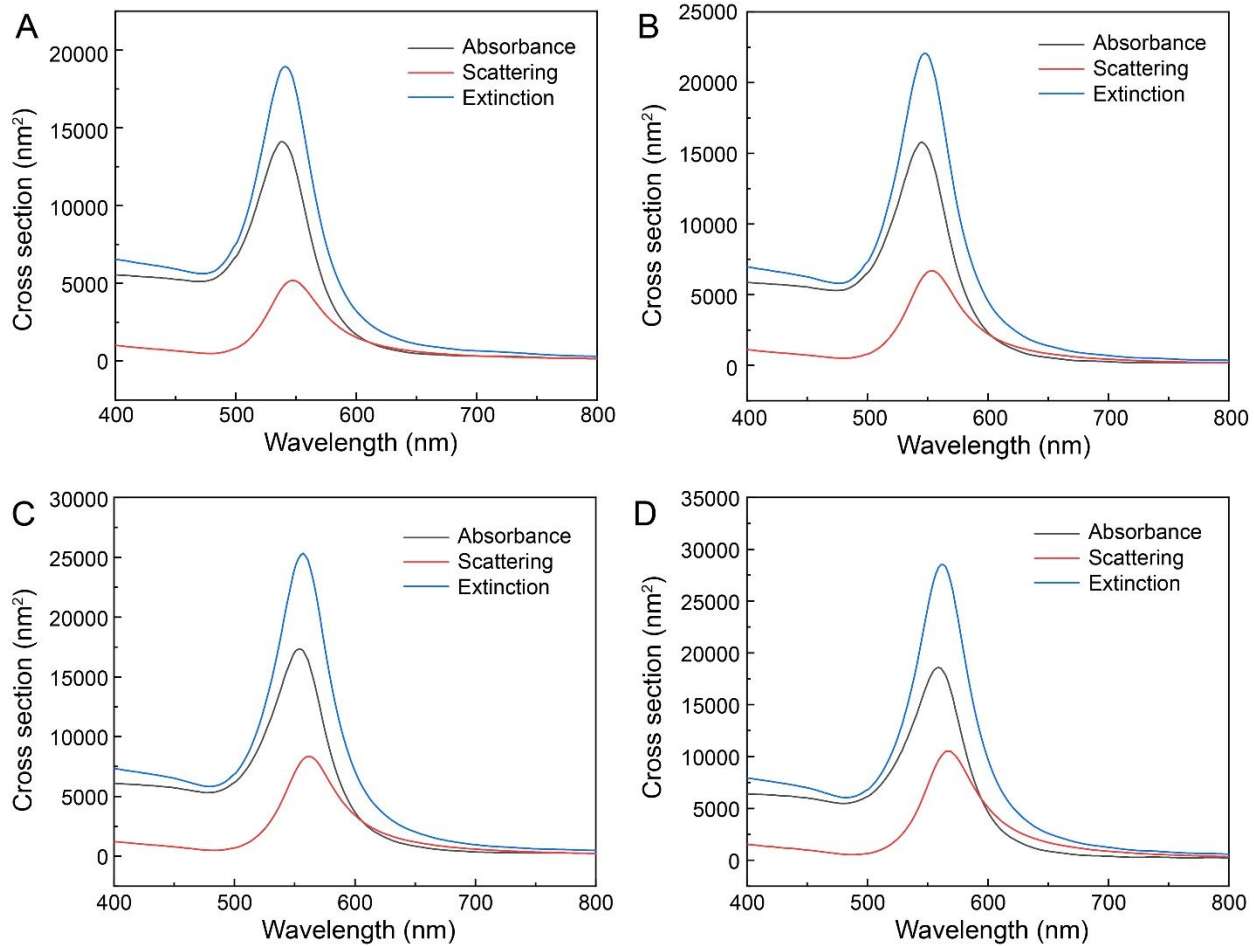


Fig. S6.

Simulated absorbance, scattering, and extinction spectra of the Janus Au-pBDT patchy nanoparticles with different size of patch: 0 nm (A), 2 nm (B), 20 nm (C), and 40 nm (D).

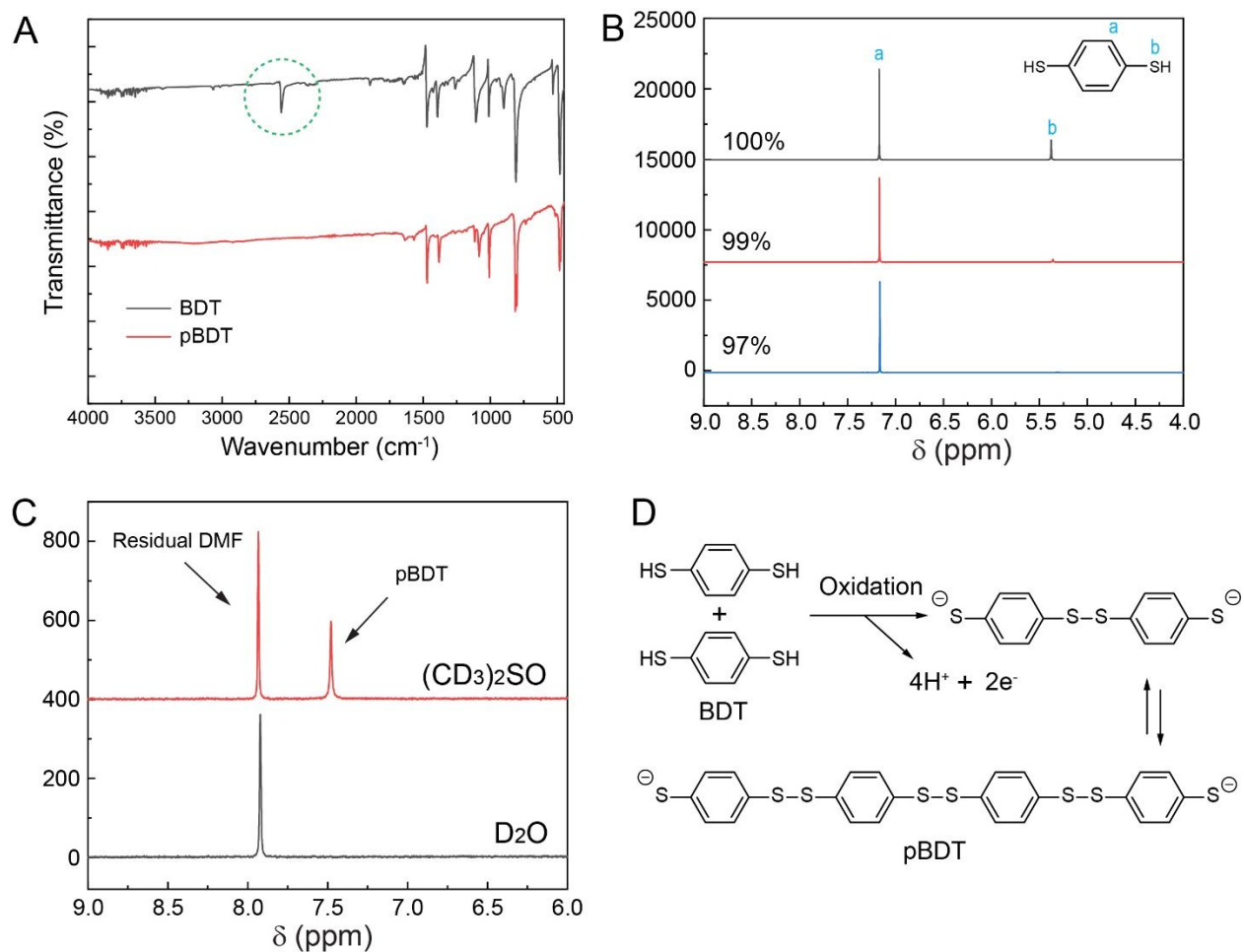


Fig. S7.

(A) FTIR spectra of BDT and pBDT. The result showed the disappearance of the $\nu_{\text{S-H}}$ stretching mode at 2559 cm^{-1} (green circle) indicating linkage of the thiol groups and polymerization of BDT. (B) ^1H NMR (300 MHz, $(\text{CD}_3)_2\text{SO}$, 298 K) of BDT in $(\text{CD}_3)_2\text{SO}$ - D_2O two-component solvent with different volume ratios of $(\text{CD}_3)_2\text{SO}$ from 100% (top) to 97% (bottom). A decrease of thiol group signal in proton NMR can be observed with increased D_2O suggesting the obvious deprotonation of thiol groups in aqueous environment. (C) ^1H NMR (300 MHz, 298 K) of Janus nanoparticles in D_2O (bottom) and $(\text{CD}_3)_2\text{SO}$ (top). The missing proton NMR signal of pBDT in D_2O indicated the assembled phase (i.e., aggregates) of pBDT in aqueous environment. (D) The proposed polymerization mechanism between BDT molecules.

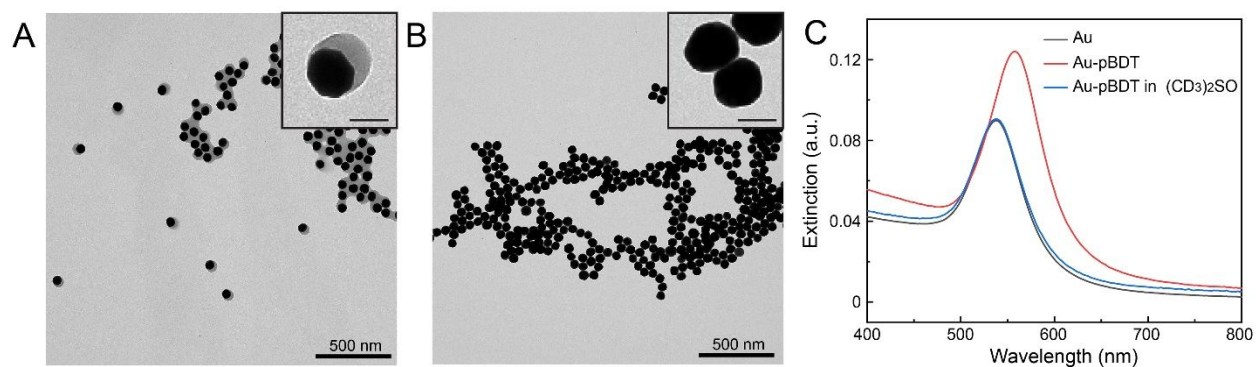


Fig. S8.

TEM images of Au-pBDT patchy nanoparticles before (A) and after (B) incubation in $(CD_3)_2SO$. (C) UV-vis extinction spectra of pristine AuNPs (black) and the Janus Au-pBDT patchy nanoparticles before (red) and after $(CD_3)_2SO$ treatment (blue). The inset TEM images confirmed the successful removal of pBDT patches on AuNPs. Scale bars in insets are 50 nm. The blue-shift and reduced extinction of Au-pBDT in $(CD_3)_2SO$ (i.e., after 1 h incubation, centrifuge, and re-disperse in water) further confirm this result. It is notable that the LSPR of Au-pBDT after $(CD_3)_2SO$ treatment was almost identical to the original AuNPs suggesting that the AuNPs were well dispersed in water without obvious aggregation.

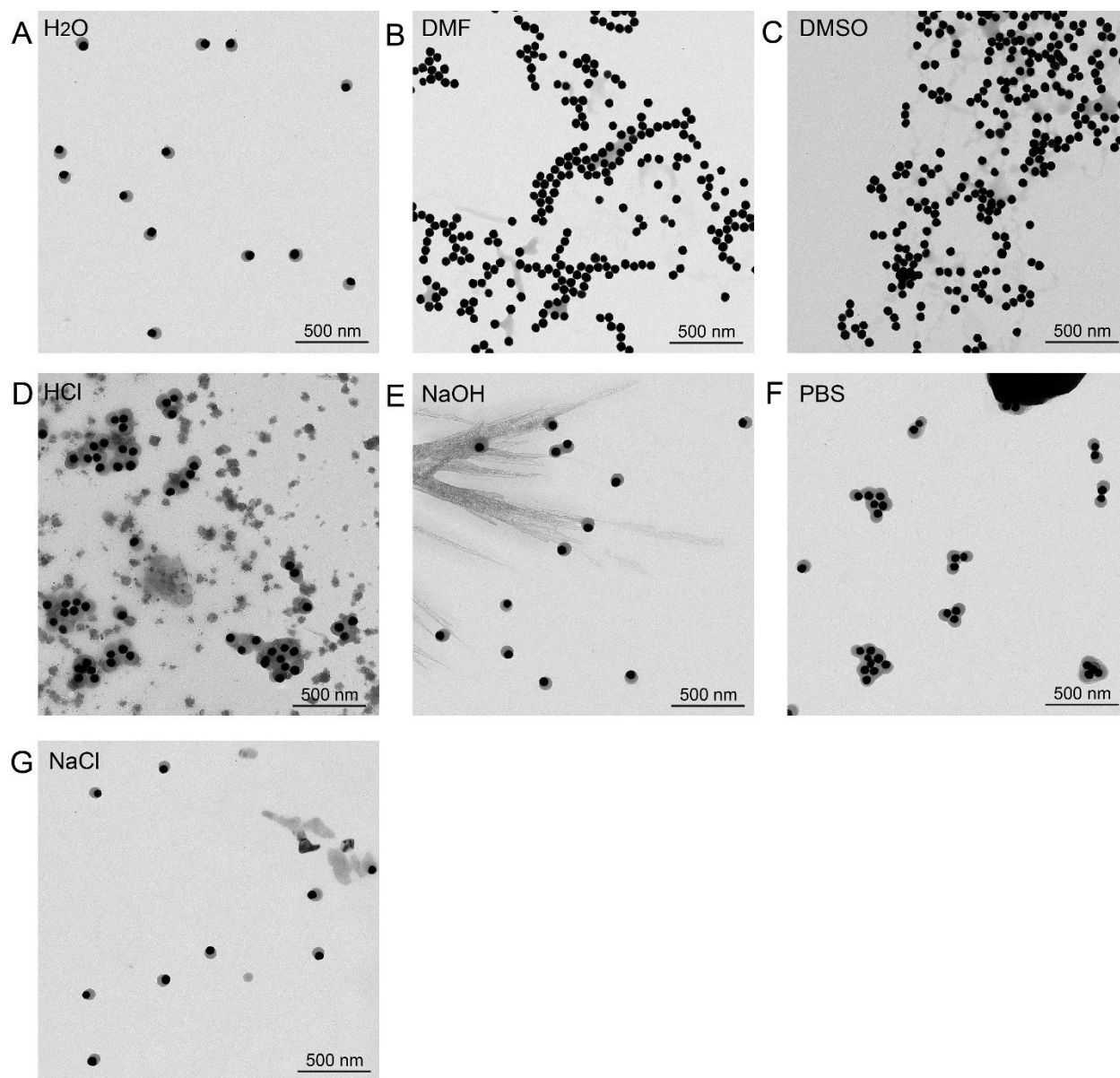


Fig. S9.

Stability of the Janus Au-pBDT patchy nanoparticles in different solvent or media for 1 h: Janus Au-pBDT patchy nanoparticles in water (A), DMF (B), DMSO (C), 20 mM HCl (D), 20 mM NaOH (E), 1 × PBS (F), and 100 mM NaCl (G), respectively. All the samples were collected by centrifuging one time and resuspending in water followed by casting on TEM grids for characterization. The results suggested that the pBDT can easily disassemble in organic solvent (e.g., DMF and DMSO). However, these structures largely retained their structure integrity in diverse aqueous environment including extreme pH and high ionic strength.

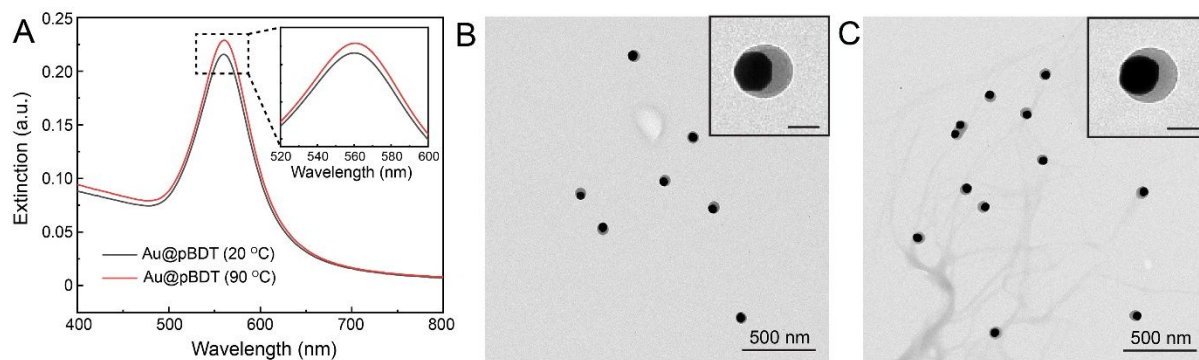


Fig. S10.

The stability of Janus Au-pBDT nanoparticles at high temperature (i.e., 90 °C). (A) UV-vis extinction spectra of the Janus Au-pBDT patchy nanoparticles before and after 3 h incubation at 90 °C. TEM images the Janus Au-pBDT patchy nanoparticles before (B) and after (C) thermal treatment. Scale bars in insets are 50 nm. Both spectra exhibited an almost identical LSPR peak indicating the monodisperse nature of the products and the complete structure of the patches. This is also confirmed by TEM images where the morphologies of the patchy nanoparticles were the same.

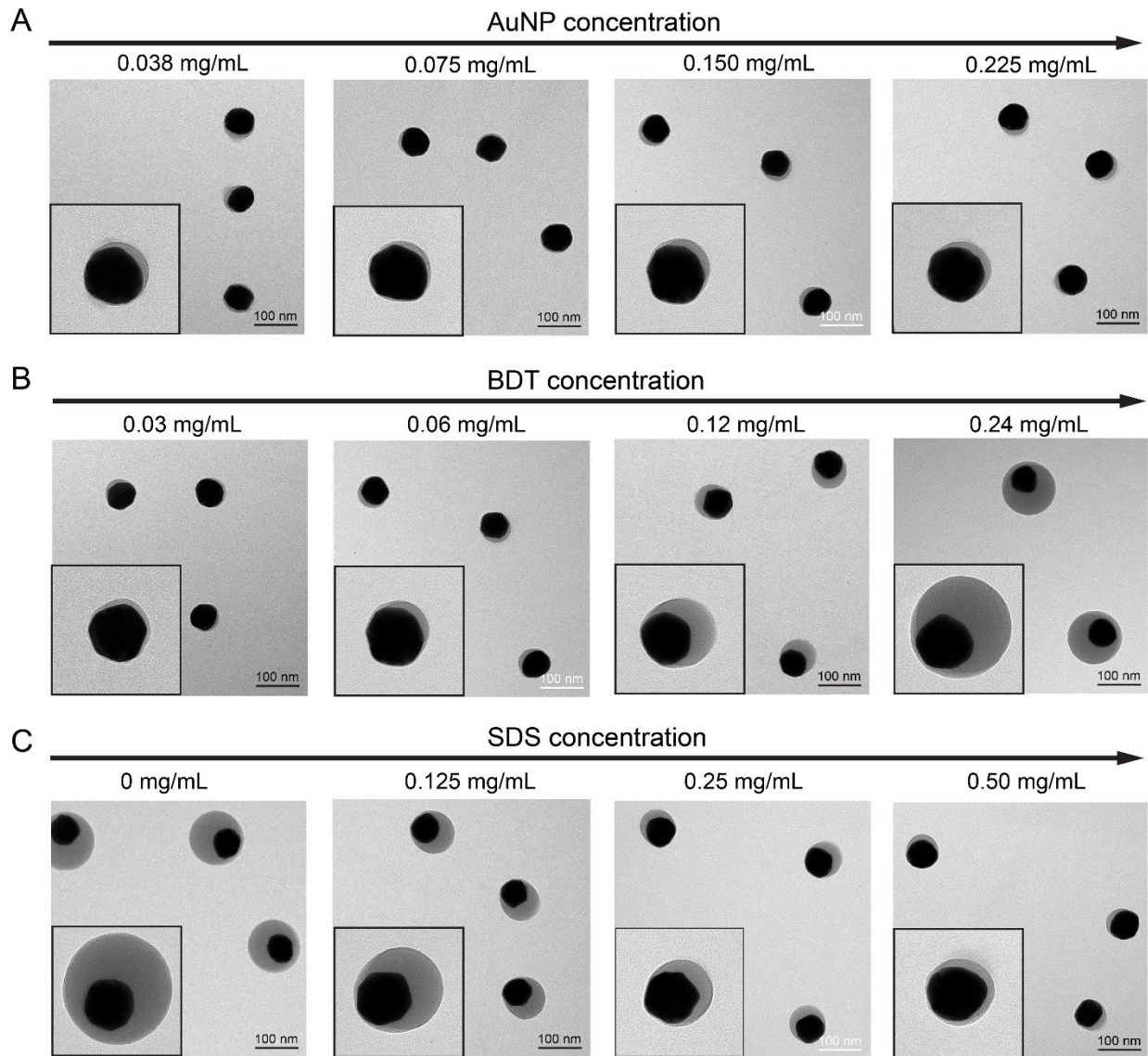


Fig. S11.

TEM images of Au-pBDT patchy nanoparticles prepared by using different stoichiometries. (A) Different concentration of AuNPs with the BDT and SDS concentration at 0.06 mg mL^{-1} and 0.5 mg mL^{-1} , respectively. (B) Different concentration of BDT with AuNPs and SDS concentration at 0.15 mg mL^{-1} and 0.5 mg mL^{-1} , respectively. (C) Different concentration of SDS with AuNPs and BDT concentration at 0.15 mg mL^{-1} and 0.06 mg mL^{-1} , respectively.

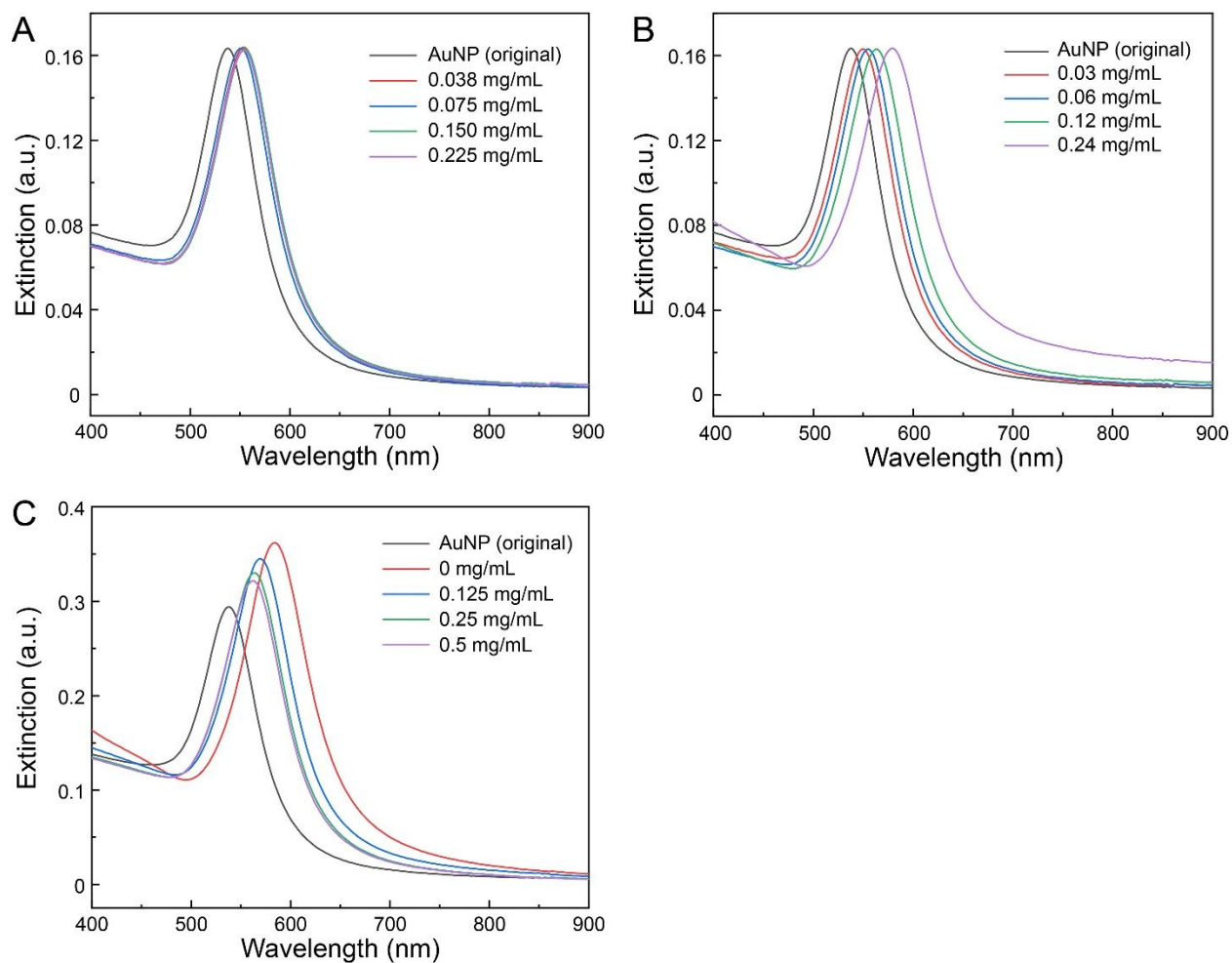


Fig. S12.

UV-vis spectra of Au-pBDT patchy nanoparticles prepared by using different stoichiometries. The narrow and single localized surface plasmon resonance (LSPR) peak indicated there is no obvious aggregation of the products.

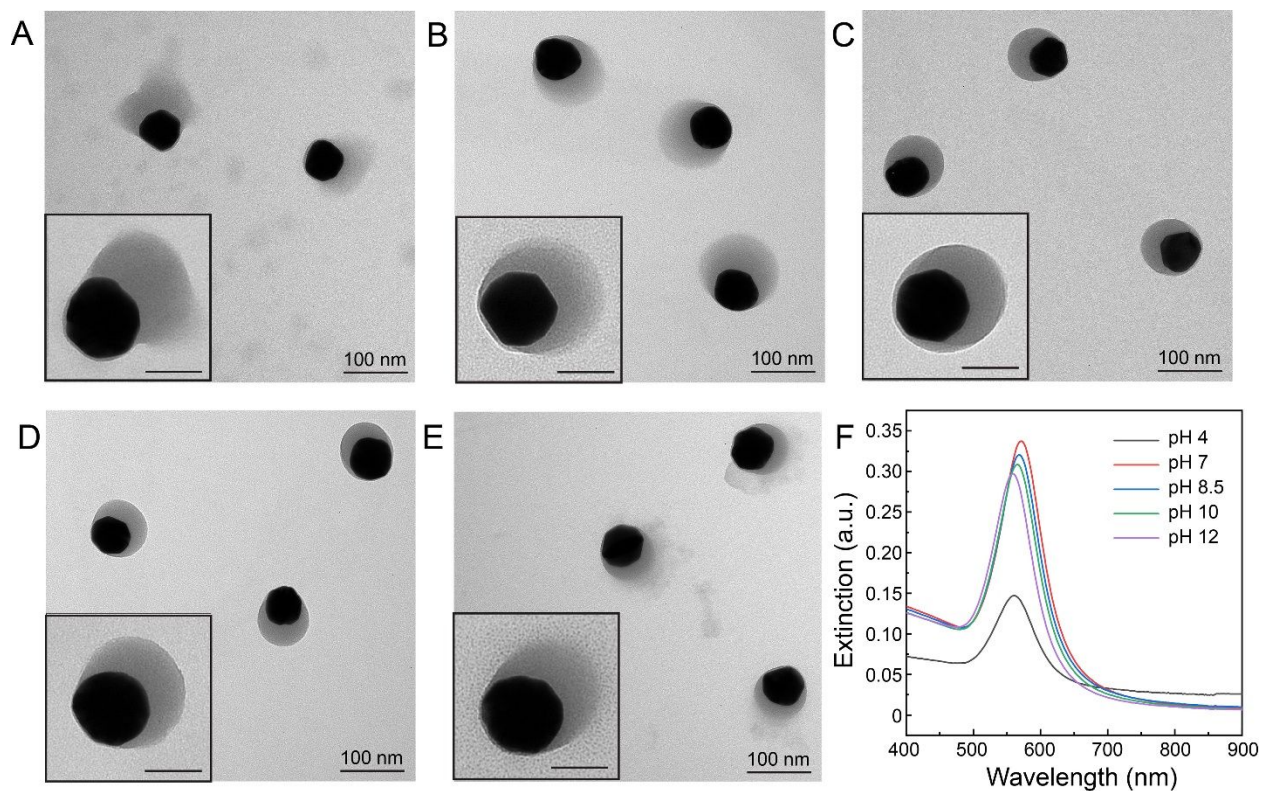


Fig. S13.

TEM images the Janus Au-pBDT patchy nanoparticles prepared at different pH values: 4 (A), 7 (B), 8.5 (C), 10 (D), and 12 (E), respectively. (F) UV-vis extinction spectra of the Janus Au-pBDT patchy nanoparticles prepared at different pH values. Insets are the close-up TEM image of representative Au-pBDT patchy nanoparticles; scale bars are 50 nm. All the TEM images showed the Janus structure of the patchy nanoparticles. In basic environment (e.g., pH 7-12), the quality of the patchy nanoparticles looked almost identical to baseline conditions. In contrast, there were many patch fragments in acid environment (e.g., pH 4) and a considerable aggregation of AuNPs due to the low yield of the products (black line in **Fig. S13F**). We reason that the basic environment will facilitate deprotonation of thiol groups and improve the solubility of BDT in the reaction solution thus making the pBDT assembly uniform on the surface of Au. In contrast, BDT is less soluble in acidic environments leading to irregular aggregates that form immediately once added to the reaction solution.

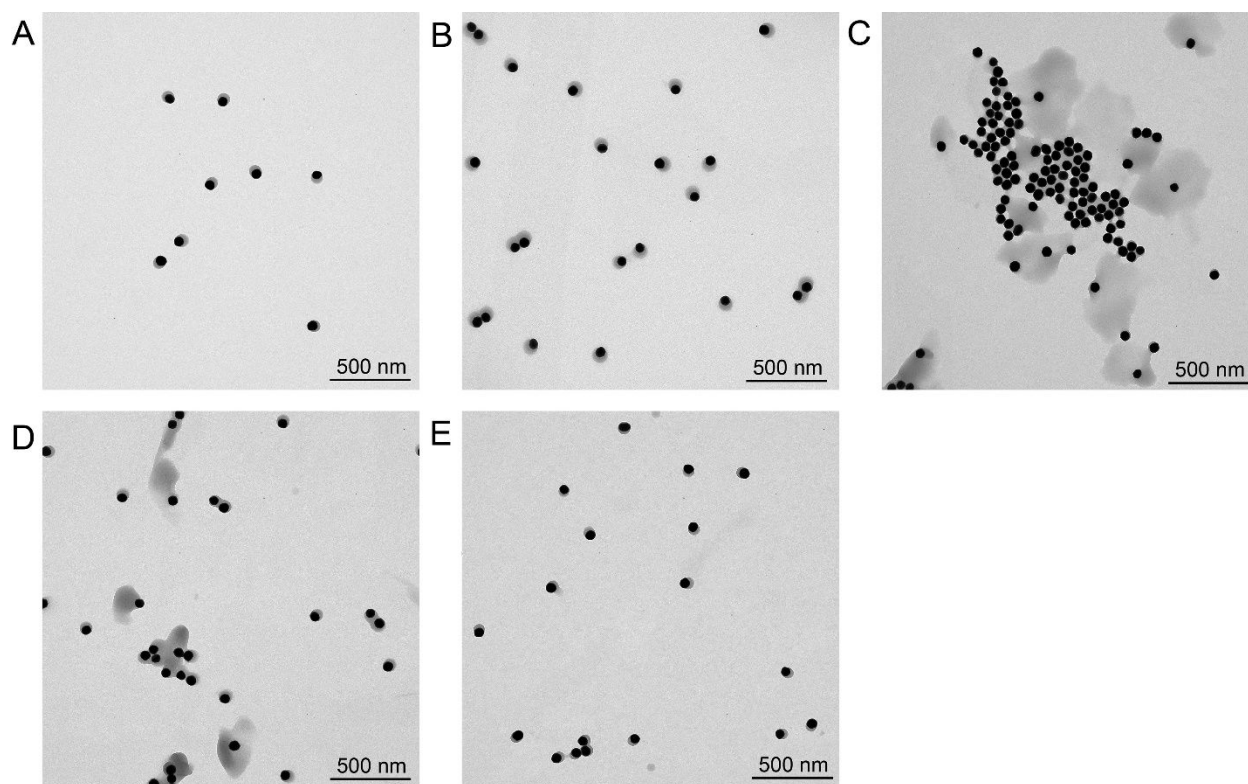


Fig. S14.

TEM images the Janus Au-pBDT nanoparticles prepared at different mediums: bicine buffer (pH 8.5) (A), TRIS buffer (pH 8.5) (B), NaOH solution (pH 8.5) (C), NaOH solution (pH 10) (D), and NaOH solution (pH 12) (E), respectively. TEM results suggested that the type of buffer did not alter the Janus patchy nanoparticles. The presence of polymeric sheet-like aggregates resulted from the aggregation of BDT and/or pBDT, as the pH value of the NaOH solution (i.e., pH 8.5 and 10) decreased to ~ 7 due to the consumption of OH^- during the reaction. Even though the pH buffer capacity of pH 12 NaOH solution is also low, the pH remained above 8 after 24 h of reaction allowing for decent solubility of BDT and/or pBDT during the assembly process.

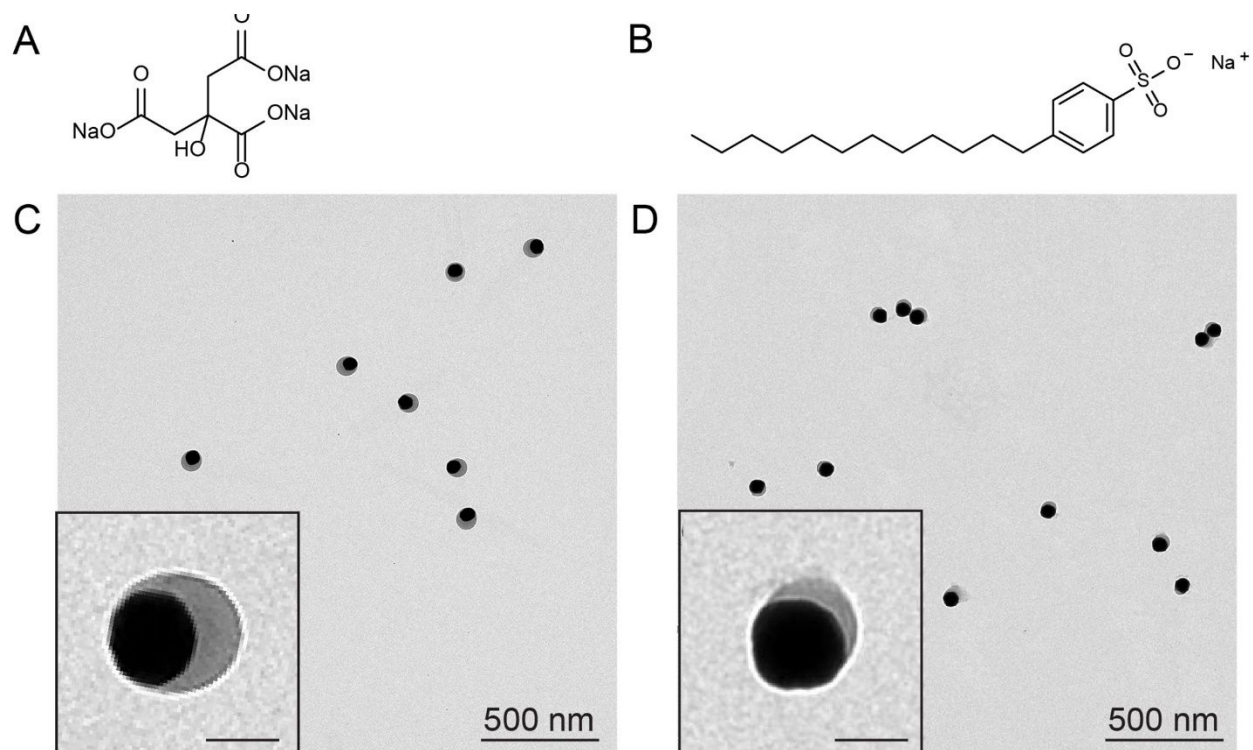


Fig. S15.

Chemical structure of different surface stabilizer: (A) sodium citrate (SC) and (B) sodium dodecylbenzenesulfonate (SDBS). TEM images the Janus Au-pBDT patchy nanoparticles prepared with same mass concentration (0.125 mg mL^{-1}). While other conditions were same, the patches prepared by SDBS were much smaller than the SC-mediated patch (20 nm v.s. 40 nm).

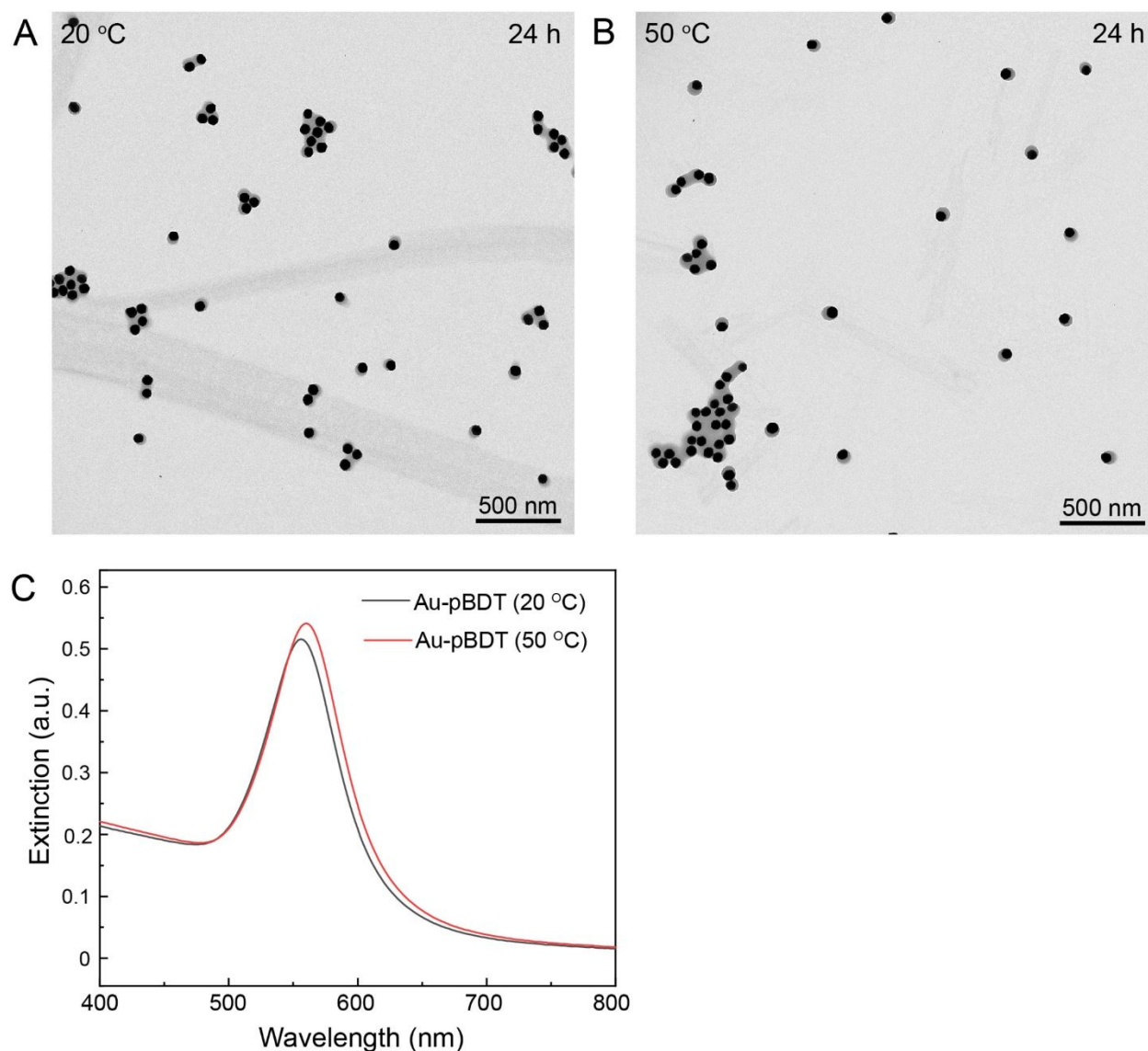


Fig. S16.

TEM images the Janus Au-pBDT patchy nanoparticles prepared at different temperatures after 24 h: 20 °C (A) and 50 °C (B), respectively. (C) UV-vis extinction spectra of the Janus Au-pBDT patchy nanoparticles prepared at different temperature after 24 h. Both spectra exhibited a narrow and single localized surface plasmon resonance (LSPR) peak indicating the monodisperse nature of the products. The LSPR of Janus nanoparticles obtained at higher temperature (i.e., 50 °C) was a bit red-shifted due to the larger patch size versus room temperature (i.e., 20 °C). This observation is likely because higher temperature can accelerate the reaction.

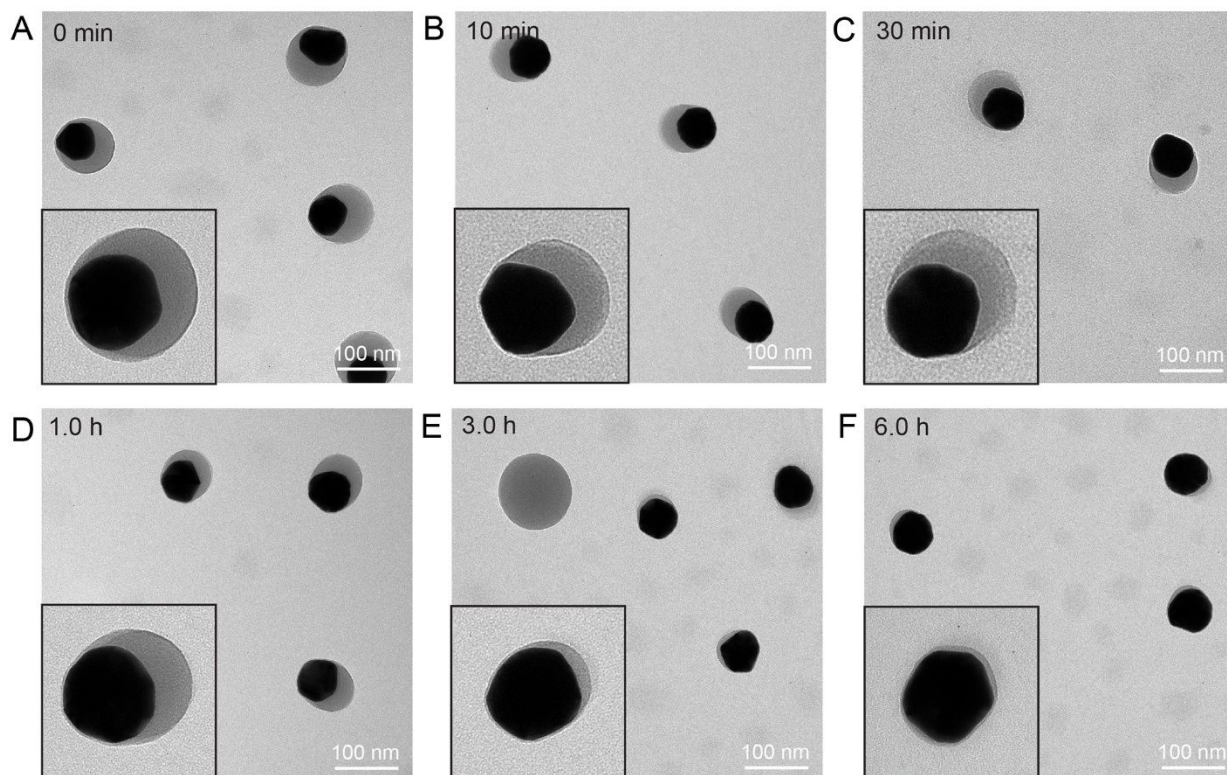


Fig. S17.

TEM images the Janus Au-pBDT patchy nanoparticles prepared with different time intervals between the addition of BDT and the addition of AuNPs: 0 min (A), 10 min (B), 30 min (C), 1 h (D), 3 h (E) and 6 h (F), respectively. Insets are the close-up TEM image of representative Au-pBDT patchy nanoparticles. Scale bars in inserts are 50 nm. All the TEM images showed the Janus structure of the patch nanoparticles. We reason that the polymerization of BDT and assembly of pBDT will occur after adding BDT into bicine buffer. If AuNPs were present in the reaction solution at the beginning of the reaction (≤ 1 h), then the BDT and/or pBDT would bind to the surface of Au and assemble into patches. If AuNPs were added after 3 h, most of reactive BDT was consumed and formed supramolecular nanoparticles in the solution. Therefore, the size of patch on Au was significantly smaller and many free pBDT nanoparticles were observed in the products. *Note:* while we found that the adding order of AuNPs and BDT did not significantly alter the Janus structure, BDT was added first *only* in this experiment to understand how long it takes to exhaust BDT in bicine buffer.

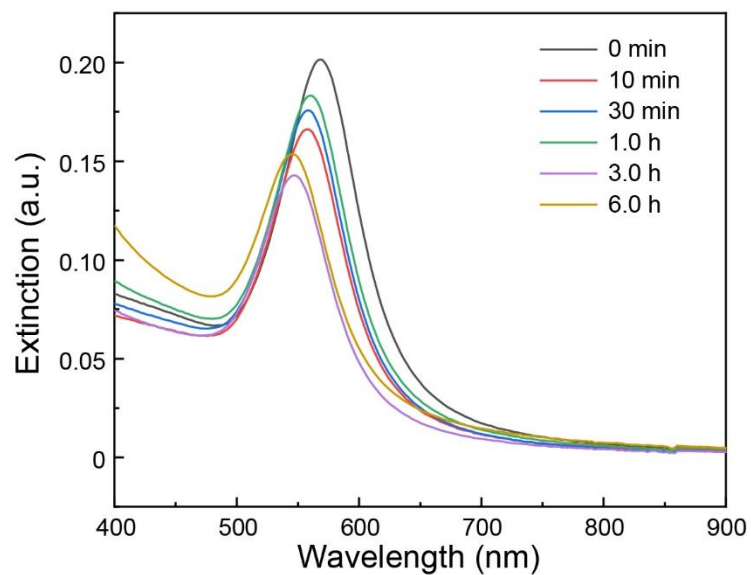


Fig. S18.

UV-vis extinction spectra of Janus Au-pBDT patchy nanoparticles prepared with different time intervals between the additional of BDT and AuNPs. The blue-shift indicated the thinner pBDT patch on AuNPs.

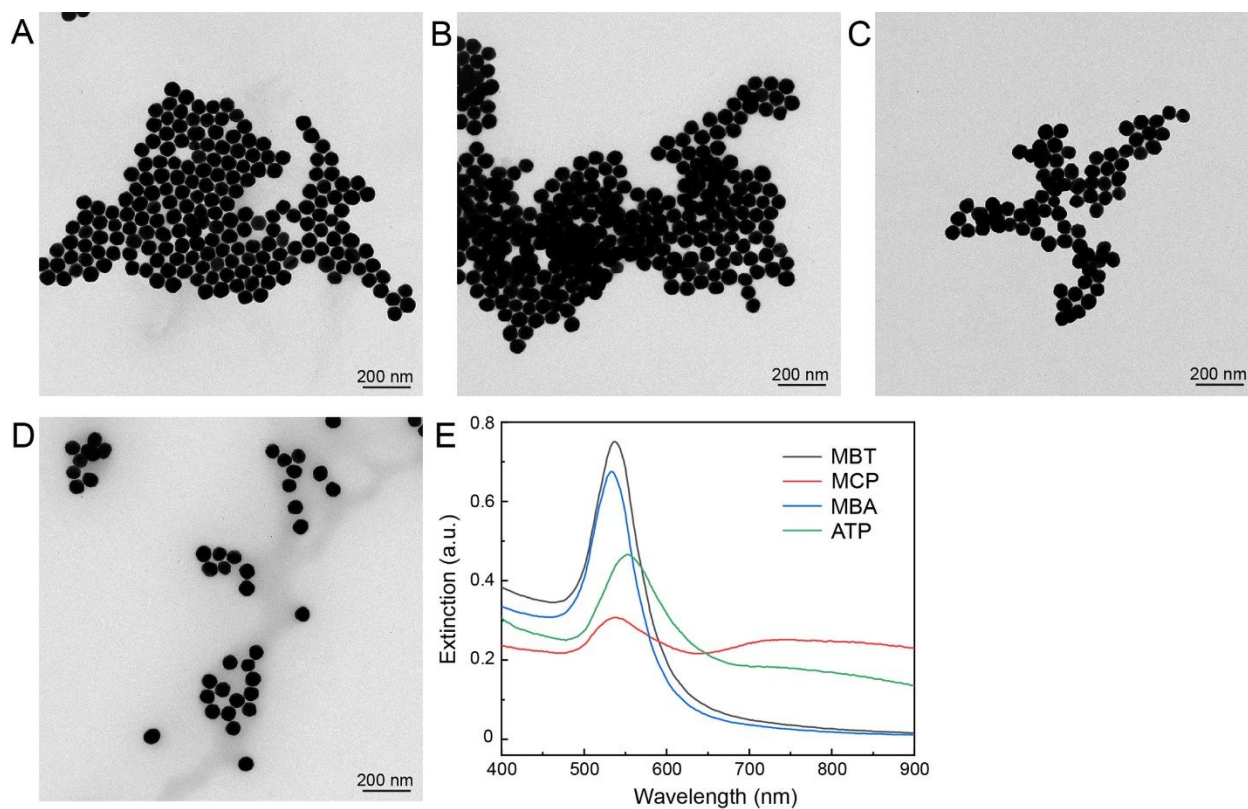


Fig. S19.

Use of mono-thiol molecules for surface coating. TEM images of AuNPs after mixing with different mono-thiol carrying molecules in bicine buffer for 20 h: MBT (A), MCP (B), MBA (C), and ATP (D), respectively. (E) UV-vis spectra of the surface-modified AuNPs. The small interparticle distance indicates the negligible thickness of coating outside the AuNPs. We reason that monothiol-carrying molecules cannot polymerize into a relative long hydrophobic chain, which is critical for the subsequent supramolecular assembly via π - π interactions.

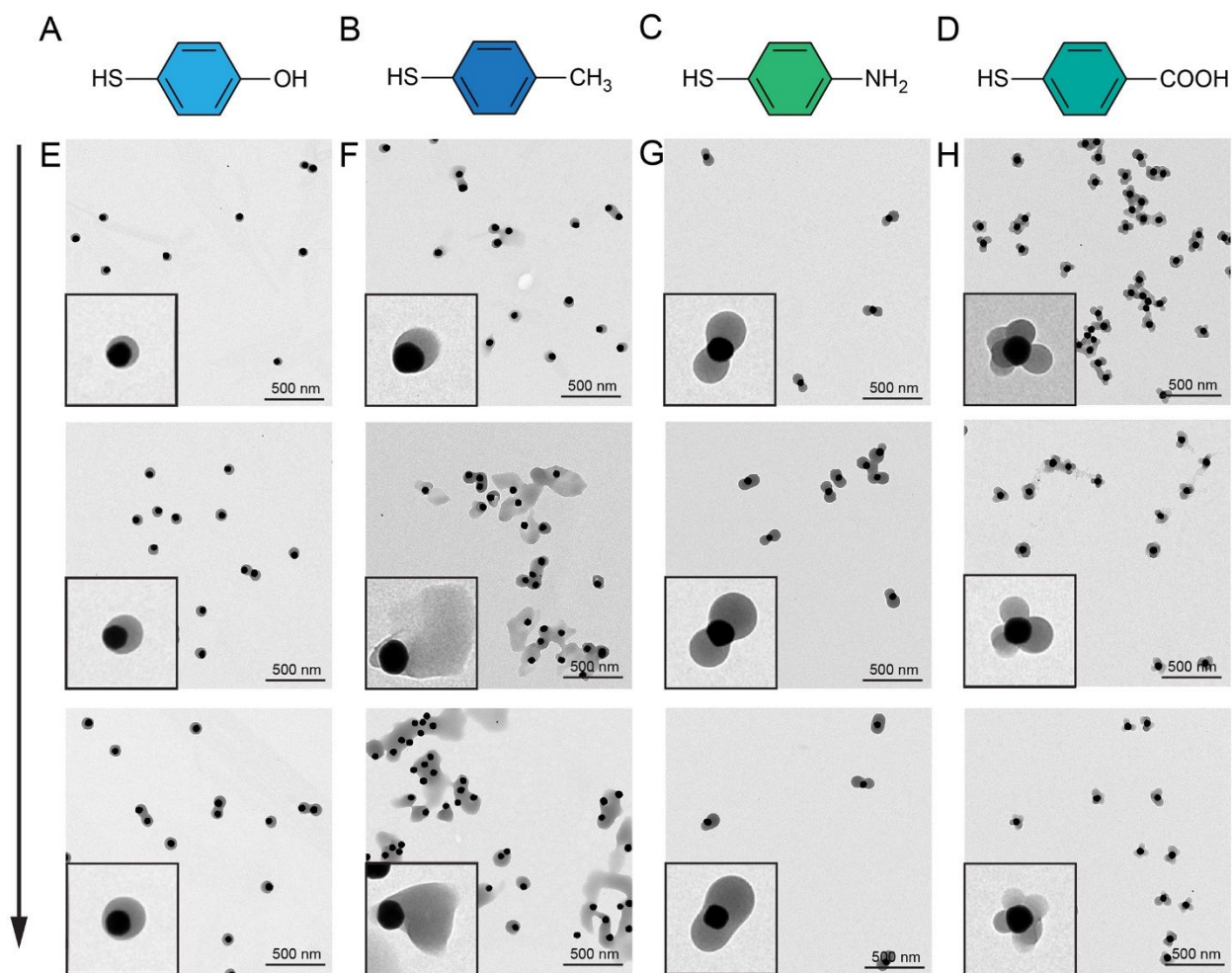


Fig. S20.

(A-D) Chemical structure of four thiol-carrying molecules used as ligand modulators in this work: MBT (A), MCP (B), MBA (C), and ATP (D), respectively. (E-H) TEM images the Janus Au-pBDT patchy nanoparticles prepared with different ratio of BDT to different ligands: MBT (E), MCP (F), MBA (G), and ATP (H), respectively. The ratio in each row is 6:1, 6:3 and 6:6, respectively (from top to bottom). The results indicated that varying the ratio in that range did not significantly change the architecture of the patchy nanoparticles except MBT. Aggregation of organic components was observed in MBT-mediated samples especially at higher MBT concentration. We reason that the poor solubility of MBT led to such aggregates.

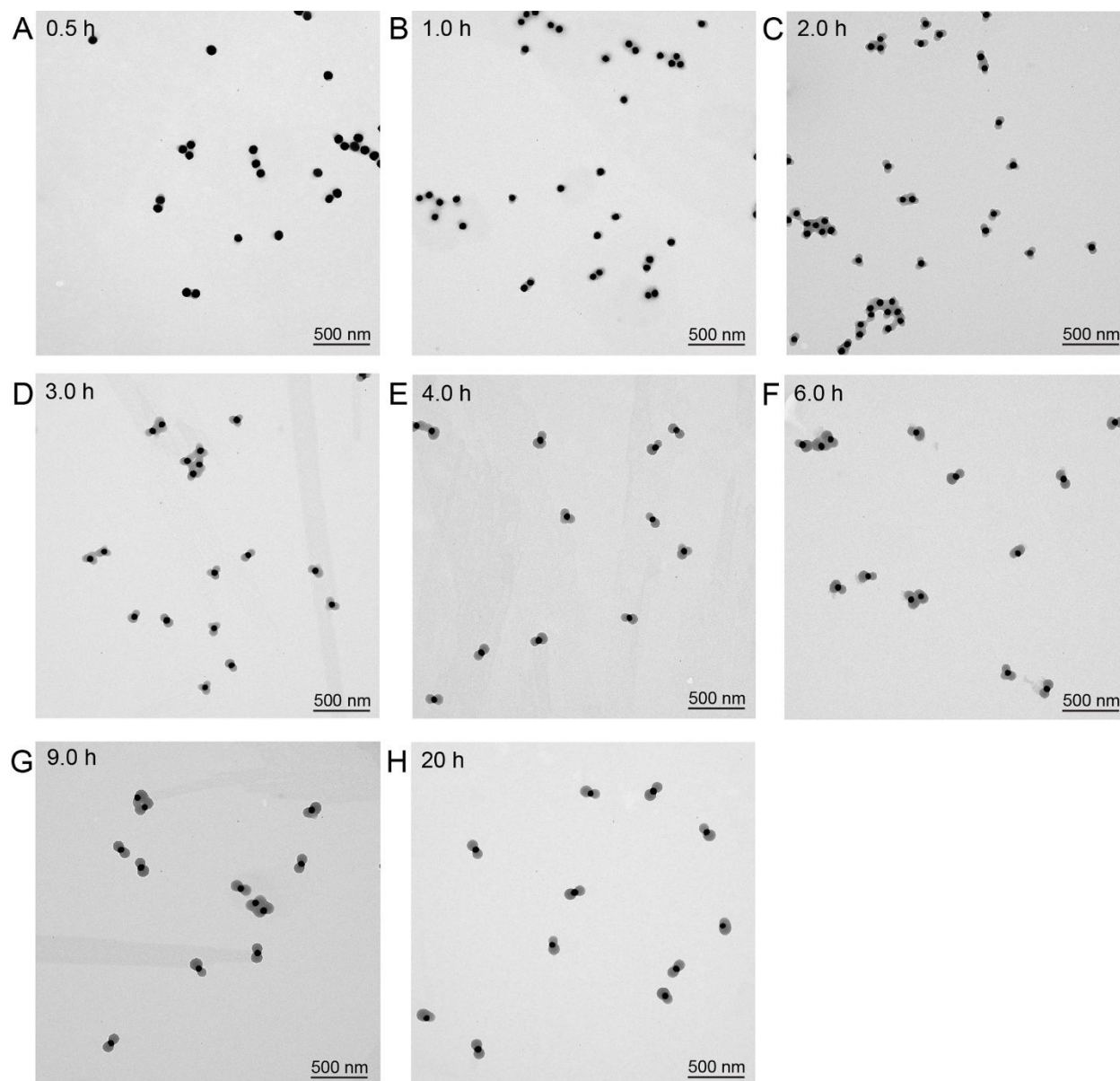


Fig. S21.

Time-dependent TEM images of Au-pBDT nanoparticles prepared with ATP. The well-defined two-patch structure on AuNP mediated by ATP provided a good platform to investigate the dynamics of the patch assembly. To obtain the samples at different time point, an aliquot of reaction solution (100 μL) was taken from the whole reaction and the assembly was quenched by adding 20-fold excess of water. Afterwards, the nanoparticles were collected by centrifugation and cast on TEM grids for analysis. The results suggested that in the first 4 h of reaction, multiple patches (i.e., more than two patches) can be observed on AuNPs. As the reaction continues, patches can reorganize and form two symmetric patches on the AuNPs.

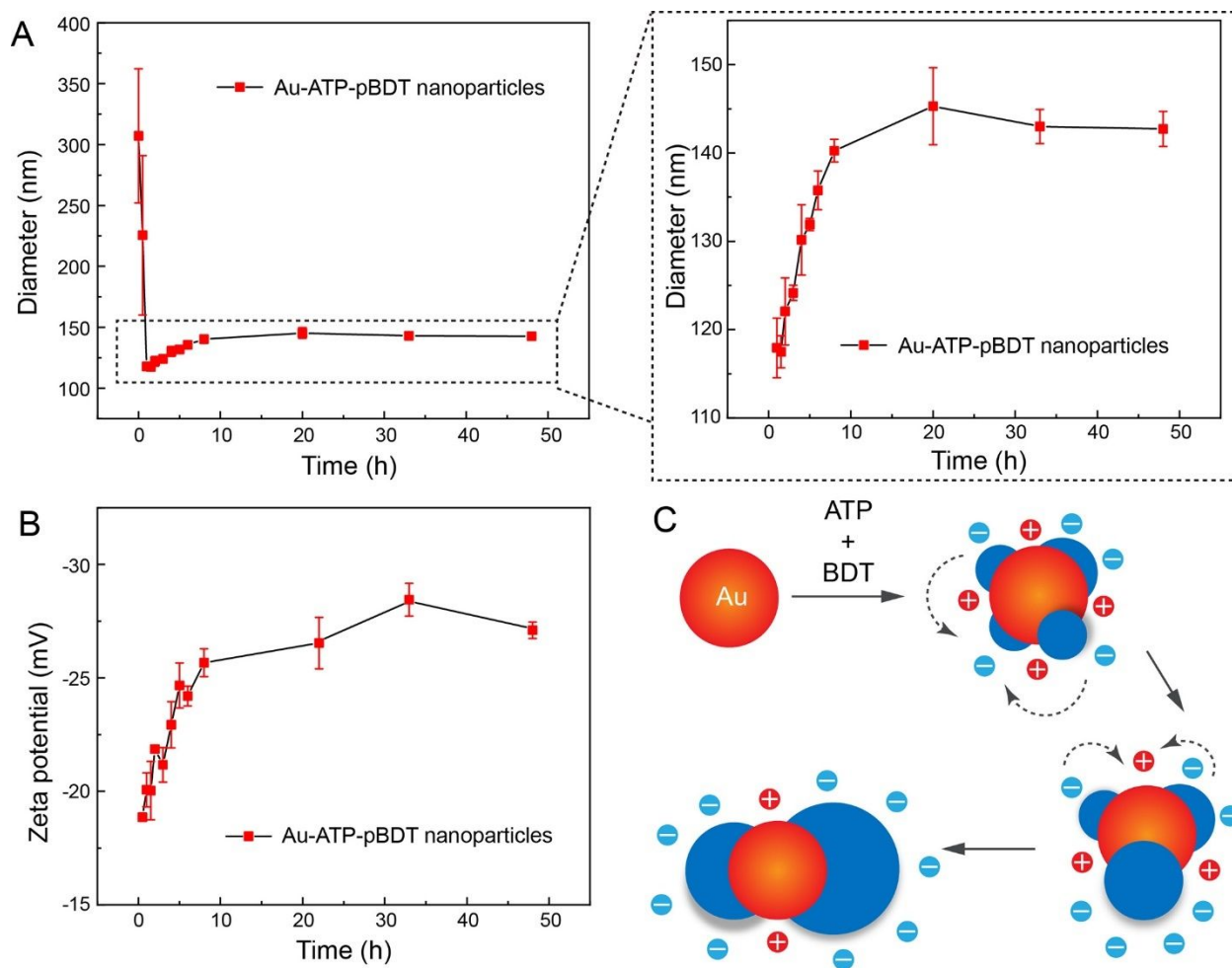


Fig. S22.

(A) DLS result of the Au-pBDT patchy nanoparticles mediated by ATP (i.e., Au-ATP-pBDT nanoparticles) collected at different time points: 5 min, 0.5 h, 1.0 h, 1.5 h, 2 h, 3 h, 4 h, 5 h, 6 h, 8 h, 20 h, 33 h, and 48 h. The close-up image shows the size growth recorded from 1.5 h. (B) Zeta potential values of Au-ATP-pBDT patchy nanoparticles at different time points in water: 0.5 h, 1.0 h, 1.5 h, 2 h, 3 h, 4 h, 5 h, 6 h, 8 h, 20 h, 33 h, and 48 h. (C) Proposed mechanisms for the dynamic transformation of patch morphology on AuNPs. Compared to Au-pBDT nanoparticles in **fig. S3**, Au-ATP-pBDT nanoparticles collected at 0.5 h are inclined to aggregate (suggesting their low colloidal stability) and the zeta potential of patchy nanoparticles keeps becoming more negative. We propose that the coulombic repulsion between different patches on a confined Au surface increases as patches grow larger (as confirmed in **fig. S22B**), which therefore limits the further growth of individual patch. To overcome this, existing small patches will dissociate and reorganize into a larger patch to lower the tension among the patches providing a morphological state of lower surface energy on patchy nanoparticles. This dynamic nature of patch formation suggests an autonomous and self-limiting assembly mechanism that balances surface binding affinity, π - π interactions, and electrostatic repulsion of the polymeric patches.

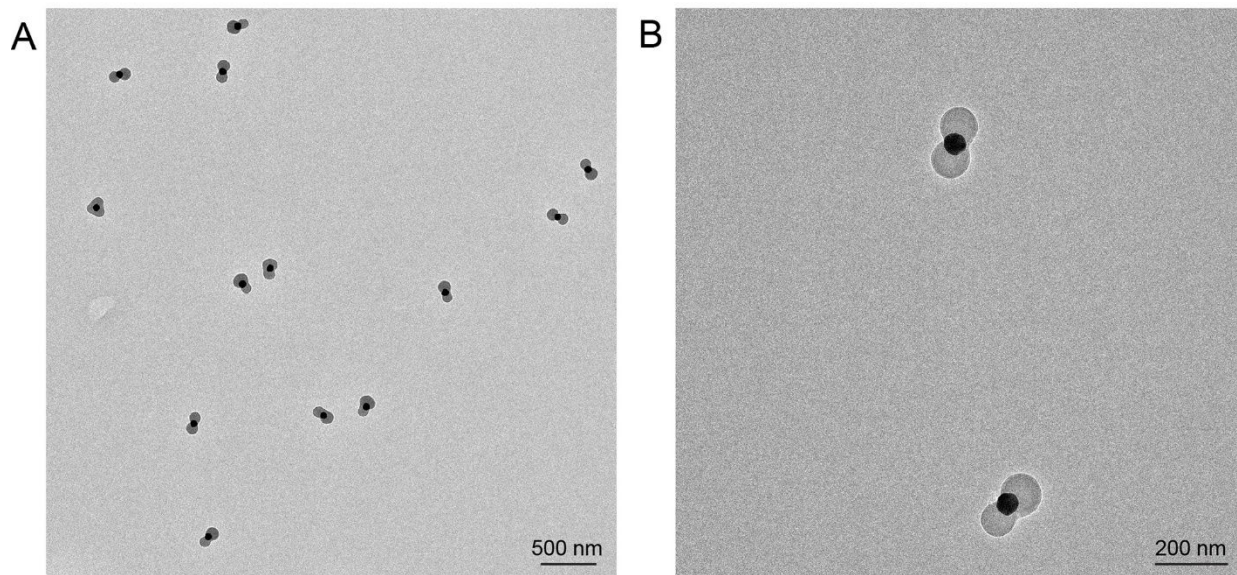


Fig. S23.

TEM images of ATP-mediated Au-pBDT nanoparticles after stored in water at room temperature (20-25 °C) for three months: (A) low and high (B) magnification of the patchy nanoparticles. The results suggested that patches on AuNPs can be maintained for a long time indicating a low total surface energy of the patchy nanosystems.

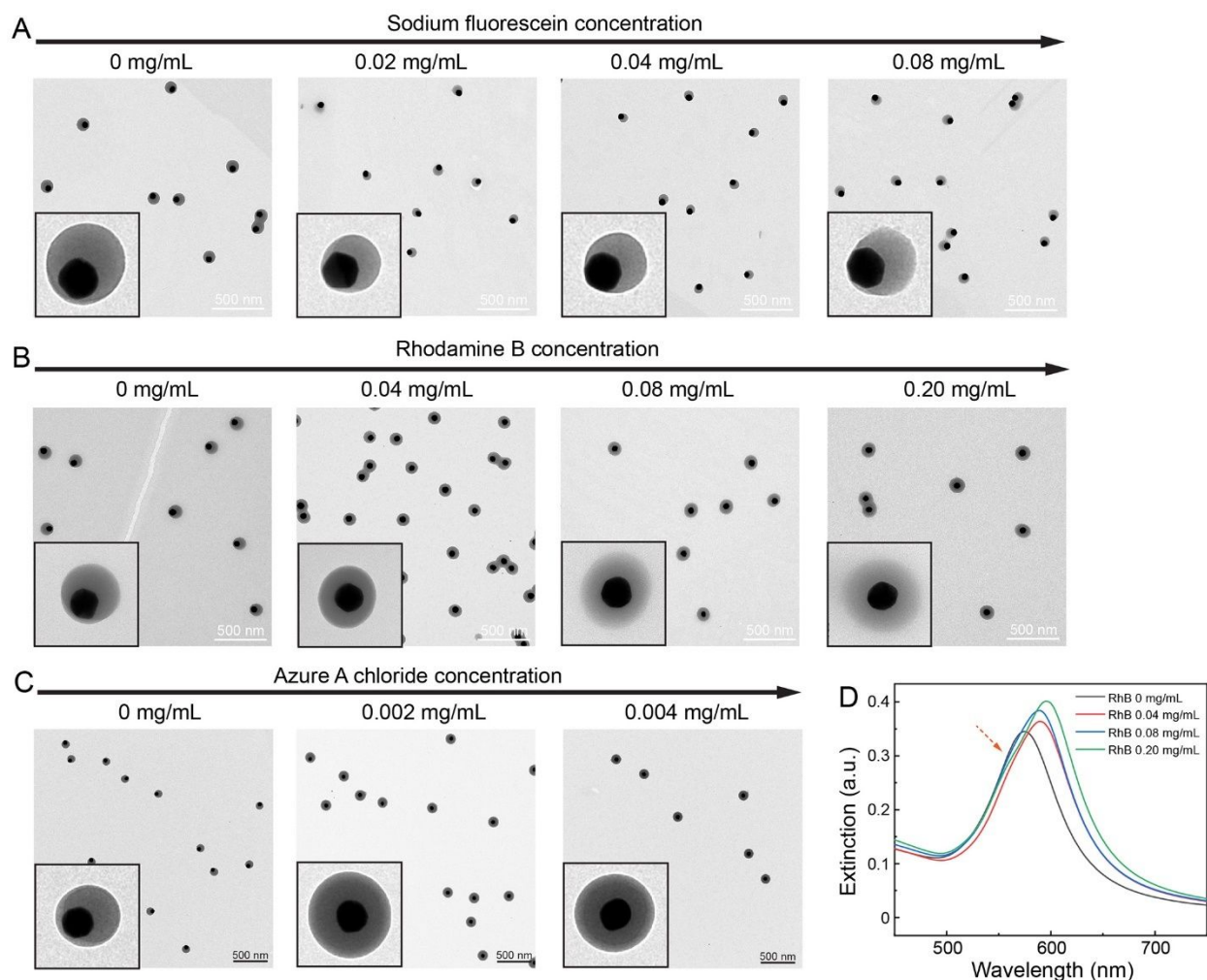


Fig. S24.

TEM image of Au-pBDT nanoparticles prepared with different dyes of varying concentrations: fluorescein sodium (molecular weight 376 Da) (A), rhodamine B (molecular weight 479 Da) (B), and azure A chloride (molecular weight 292 Da) (C), respectively. The corresponding concentration used was labeled on the top of the images. Inserts are representative images of nanoparticle from each sample. Scale bars in inserts are 50 nm. (D) UV-vis extinction spectra of Au-pBDT patchy nanoparticles prepared with different amount of RhB after centrifuging three times. The orange arrow indicates an additional shoulder absorbance, which can attribute to the integration of red RhB in the patches (*note*: we use red RhB rather than blue AAC for absorbance here because the presence of blue color from AAC may be interfered by the potential aggregation of patchy nanoparticles). For negatively charged fluorescein sodium, the morphology of the patchy nanoparticles was almost identical showing a Janus structure. In contrast, introducing RhB in the system can centralize the AuNPs even though it was still a bit off-center when the concentration of RhB was low. If a positively charged dye was used, the products exhibited a perfectly concentric core-shell nanostructure in low concentration of dye. The concentration was chosen based on our preliminary results. For example, the nanoparticles aggregated if azure A chloride concentration was 0.008 mg/mL (data not shown).

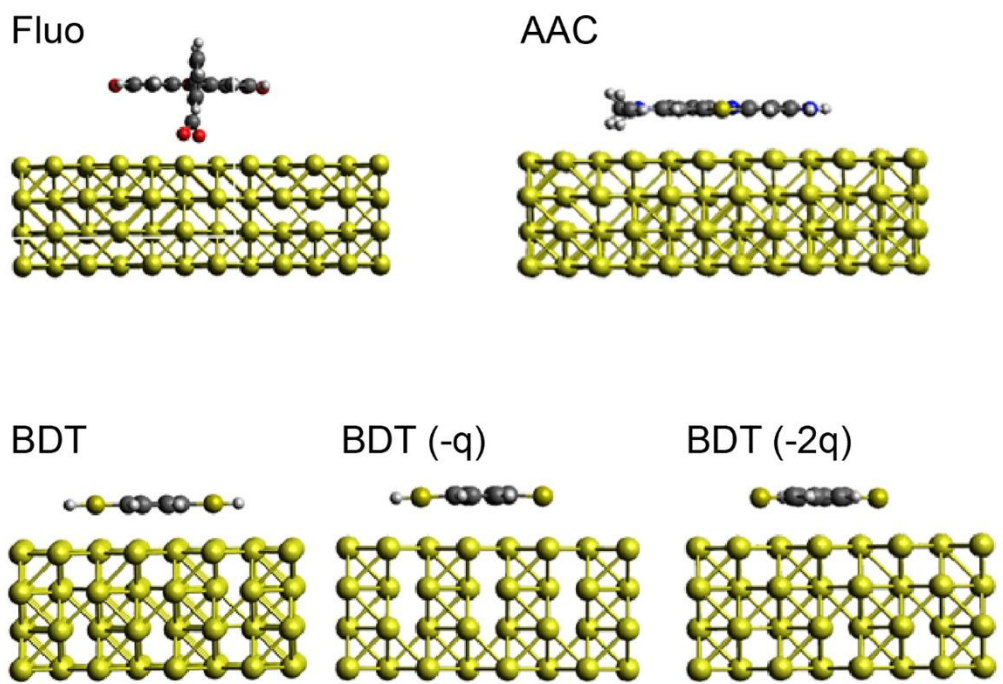


Fig. S25.
Structure of molecules used in the Siesta binding energy calculations.

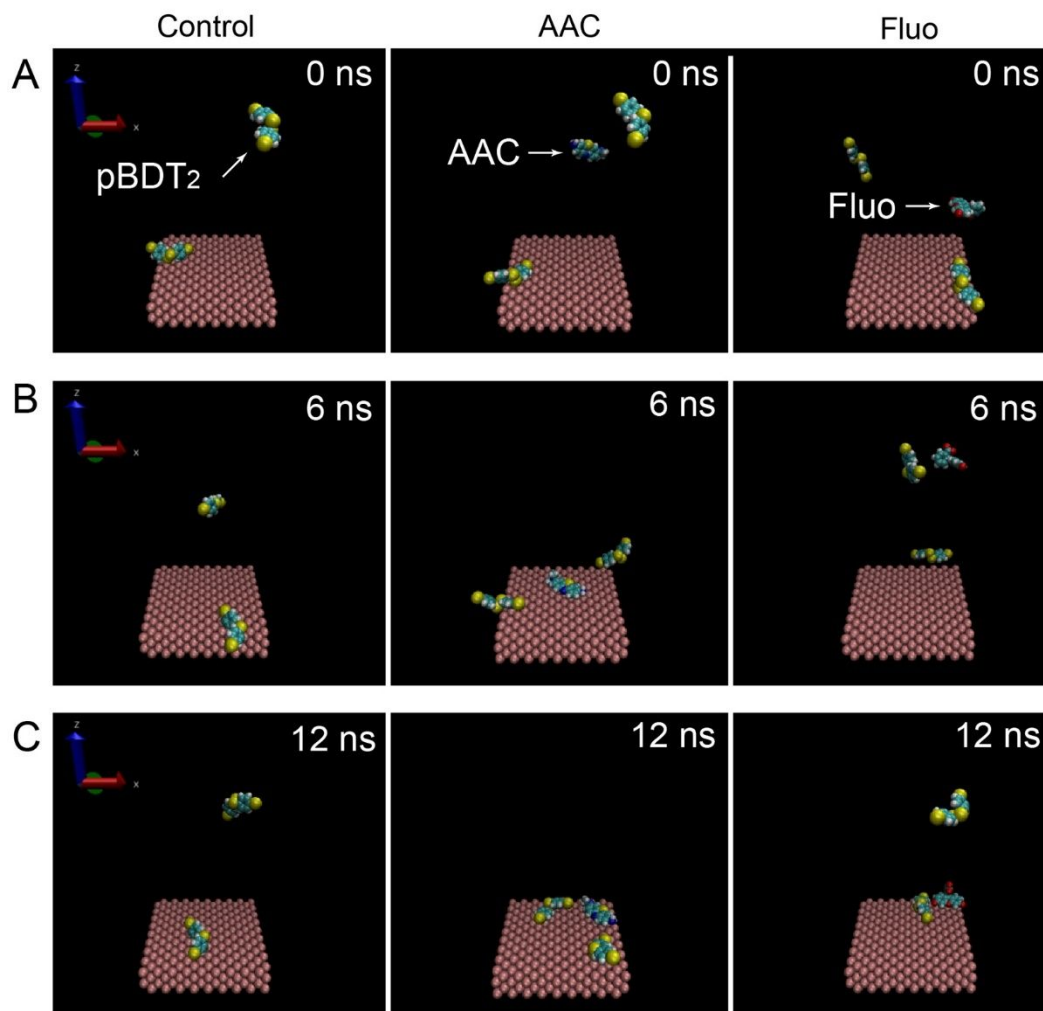


Fig. S26.

The MD snapshot of the dimer-BDT (pBDT_2), and Fluo or AAC on Au substrate (001) at 0 ns (A), 6 ns (B), and 12 ns (C) after systems were heated to 323K, respectively. The left, middle, and right figures indicated the modeling results with 2 pBDT_2 / 4 Na^+ / 2581 water/ Au-substrate, 2 pBDT_2 / 4 Na^+ / 1 AAC/ 1 Cl^- / 2556 water/ Au-substrate, and 2 pBDT_2 / 6 Na^+ / 1 Fluo/ 2552 water/ Au-substrate, respectively. The Na^+ , Cl^- , and water molecules were not shown in figures for clarity. *Note:* both pBDT_2 and pBDT_4 were used for simulation for a more conclusive mechanism for their assembly.

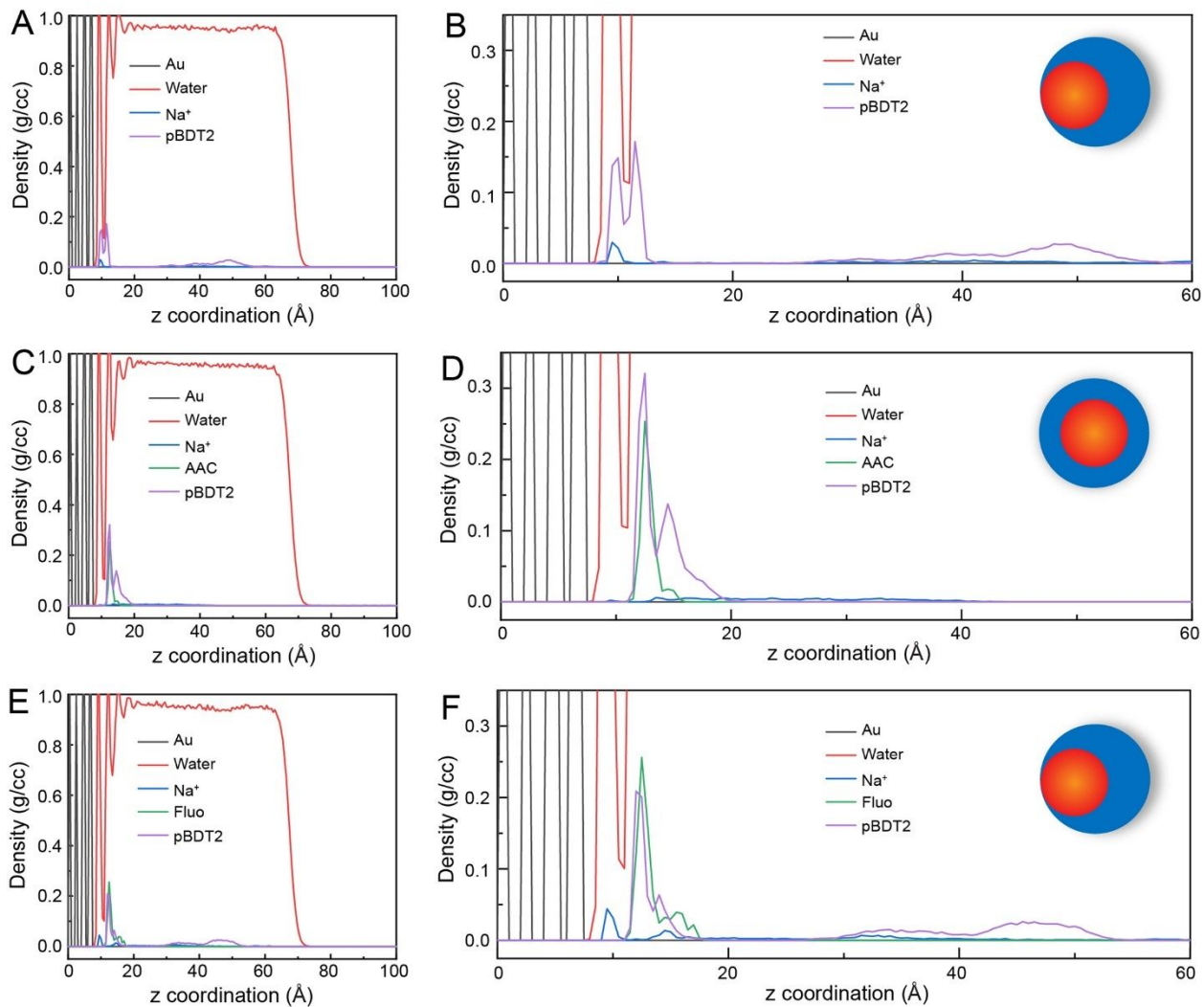


Fig. S27.

The mass density-profiles in the last 1 ns MD trajectories: 2 pBDT₂/ 4 Na⁺/ 2581 water/ Au-substrate (A), 2 pBDT₂/ 4 Na⁺/ 1 AAC/ 1 Cl⁻/ 2556 water/ Au-substrate (C), and 2 pBDT₂/ 6 Na⁺/ 1 Fluo/ 2552 water/ Au-substrate (E), respectively. The B, D, and F are the zoomed figures corresponding to A, C, and E. The Cl⁻ molecule was not shown in the figure for clarity. The results show that AAC can facilitate attachment of pBDT₂ to the surface of Au-substrate.

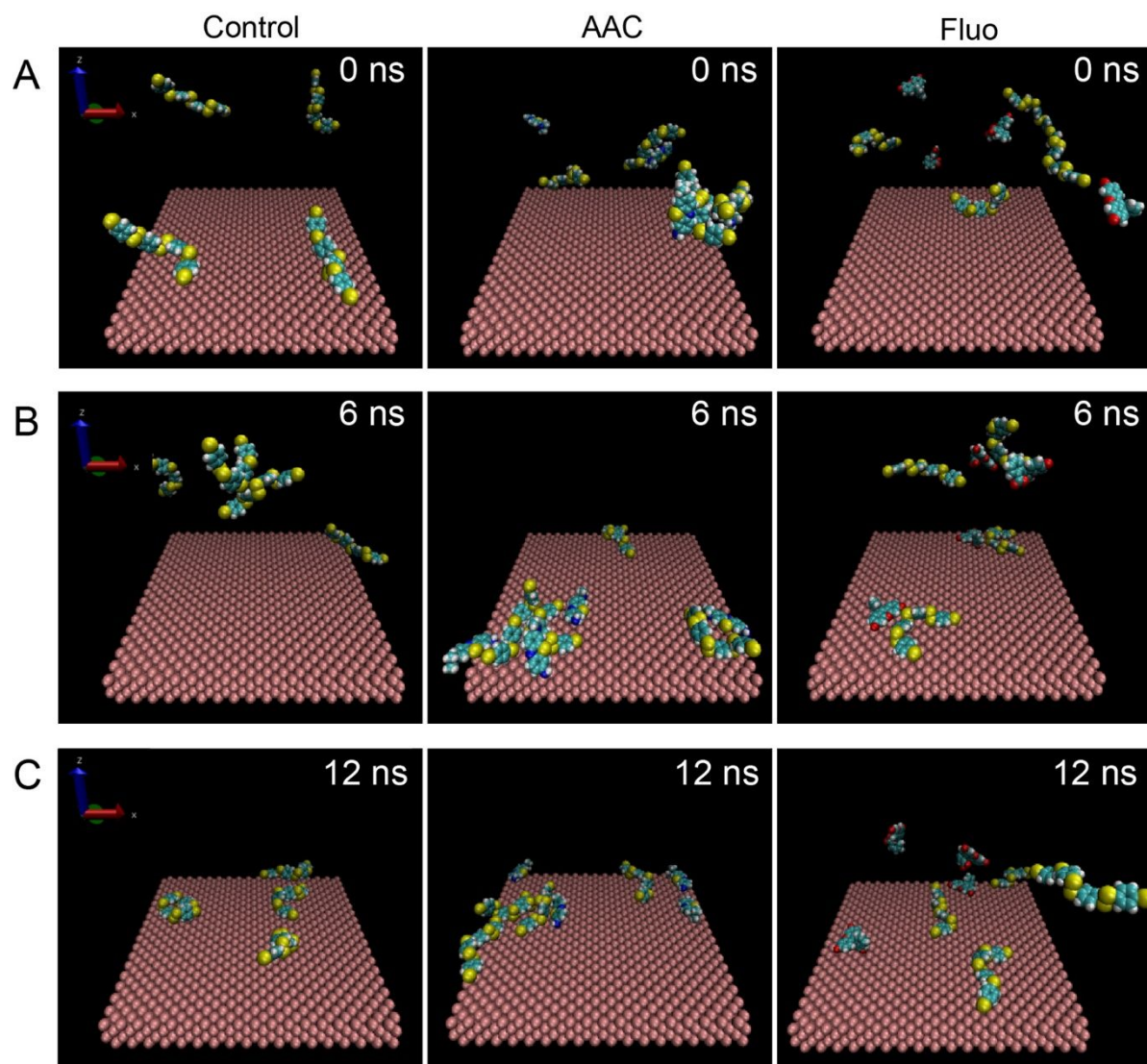


Fig. S28.

The MD snapshot of the tetramer-BDT (pBDT₄), and Fluo or AAC on Au substrate (001) at 0 ns (A), 6 ns (B), and 12 ns (C) after systems were heated to 323 K. The left, middle, and right figures indicated the modeling results with 4 pBDT₄/ 8 Na⁺/ 10336 water/ Au-substrate, 4 pBDT₄/ 8 Na⁺/ 4 AAC/ 4 Cl⁻/ 10248 water/ Au-substrate, and 4 pBDT₄/ 16 Na⁺/ 4 Fluo/ 10228 water/ Au-substrate, respectively. The Na⁺, Cl⁻, and water molecules were not shown in figures for clarity. There are many free Fluo and pBDT₄ molecules in the solution at 6 ns and 12 ns, and all of the AAC and pBDT₄ molecules were attached to the surface of Au substrate at 6 ns. AAC and pBDT₄ tends to form complexes in the solution.

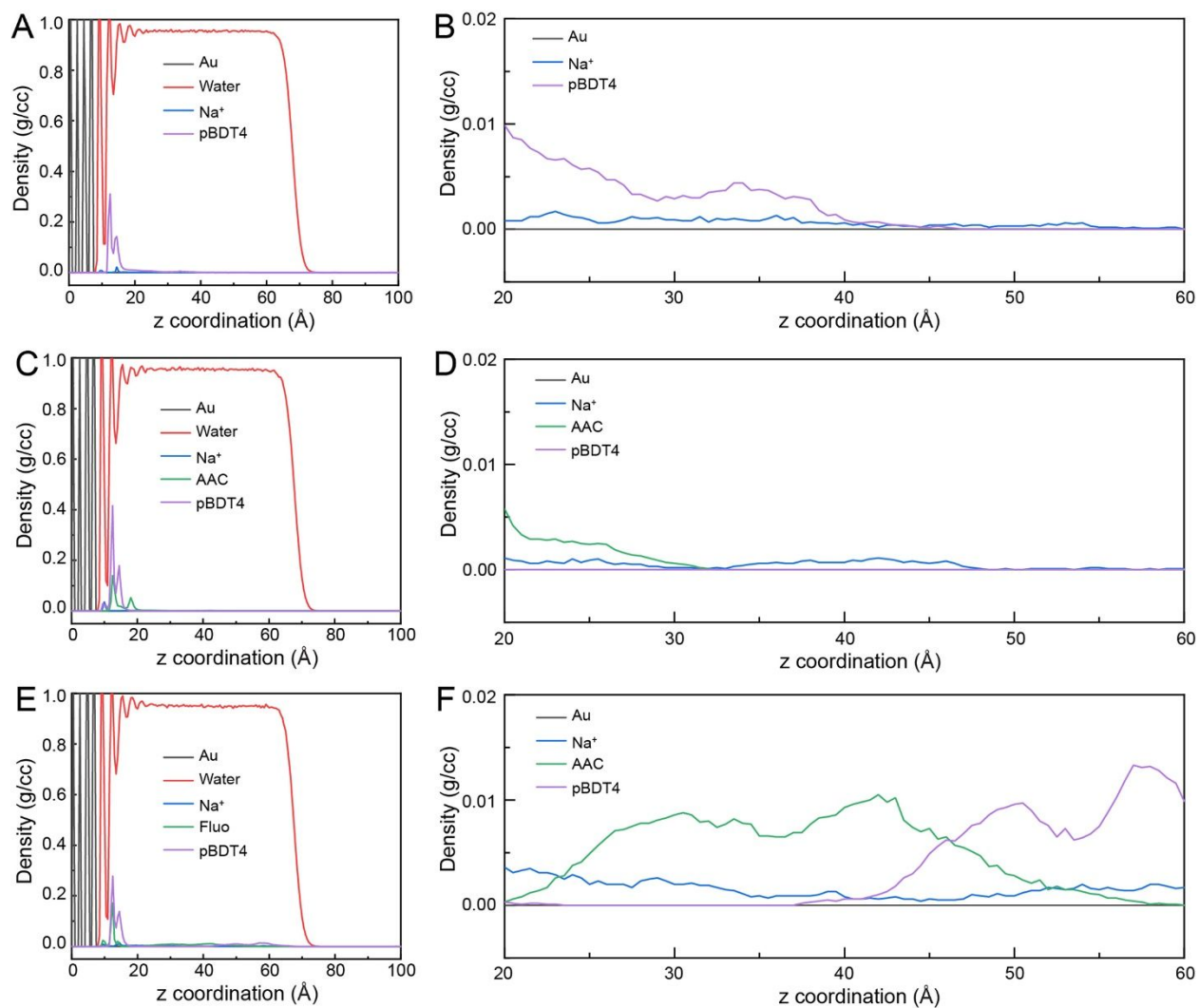


Fig. S29.

The mass density-profiles of the last 1 ns MD trajectories: (A) 4 pBDT₄/ 8 Na⁺/ 10336 water/ Au-substrate, (C) 4 pBDT₄/ 8 Na⁺/ 4 AAC/ 4Cl⁻/ 10248 water/ Au-substrate, and (E) 4 pBDT₄/ 16 Na⁺/ 4 Fluo/ 10228 water/ Au-substrate models, respectively. The B, D, and F are the zoomed figures corresponding to A, C, and E. The Cl⁻ molecules were not shown for clarity. The results show that AAC can facilitate the attachment of pBDT₄ to the surface of Au-substrate.

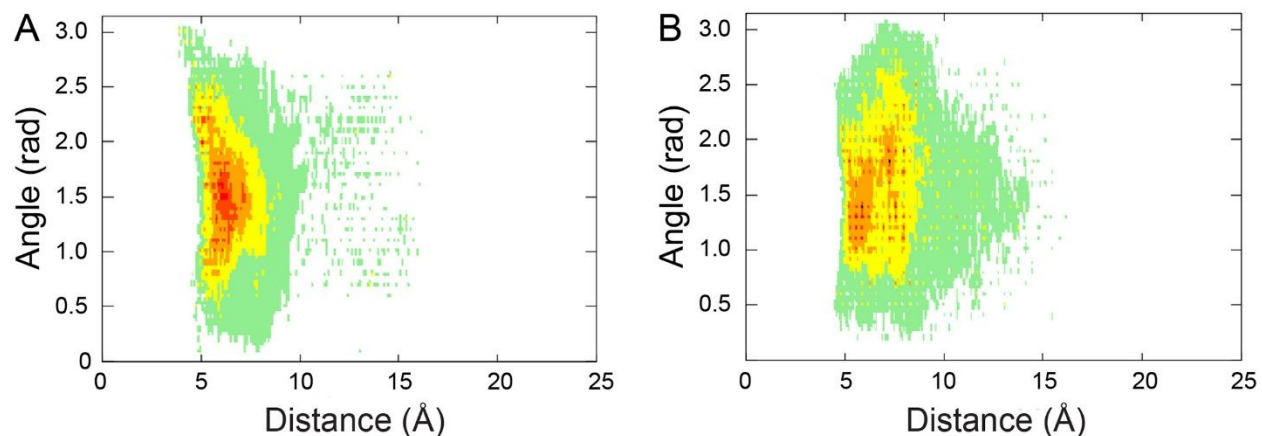


Fig. S30.

(A) Angle/distance population distribution between the planes of the aromatic rings of an AAC molecule and a pBDT₄ molecule. The system contained 1 pBDT₄, 2 Na⁺, 1 AAC, 1 Cl⁻, and 672 water molecules and was modeled at 323K. (B) Angle/distance population distribution between the planes of the aromatic rings of an Fluo molecule and a pBDT₄ molecule. The system contained 1 pBDT₄, 4 Na⁺, 1 Fluo, and 667 water molecules and was modeled at 323K. These results suggest that although the two dyes have similar aromatic structure, AAC can complex with pBDT₄ more tightly compared to Fluo. We reason that it is likely due to the positive charge of the AAC, which can preferentially interact with negative charge of pBDT₄.

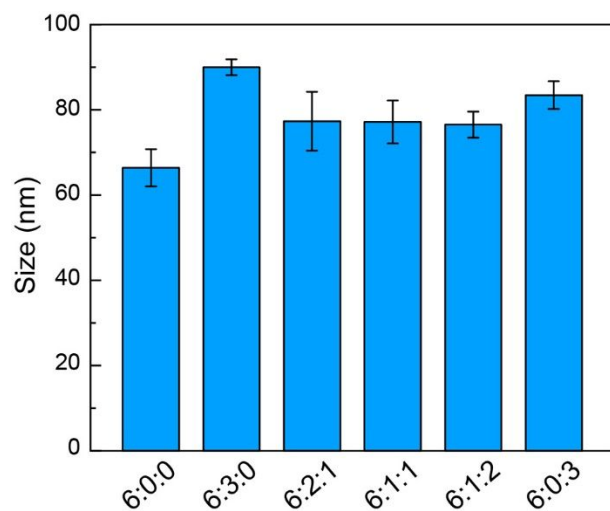


Fig. S31.

DLS results of the Au-pBDT patchy nanoparticles prepared by using ternary systems. All nanoparticles showed uniform size below 100 nm (by number weighted distribution) indicating the good monodispersity of the products.

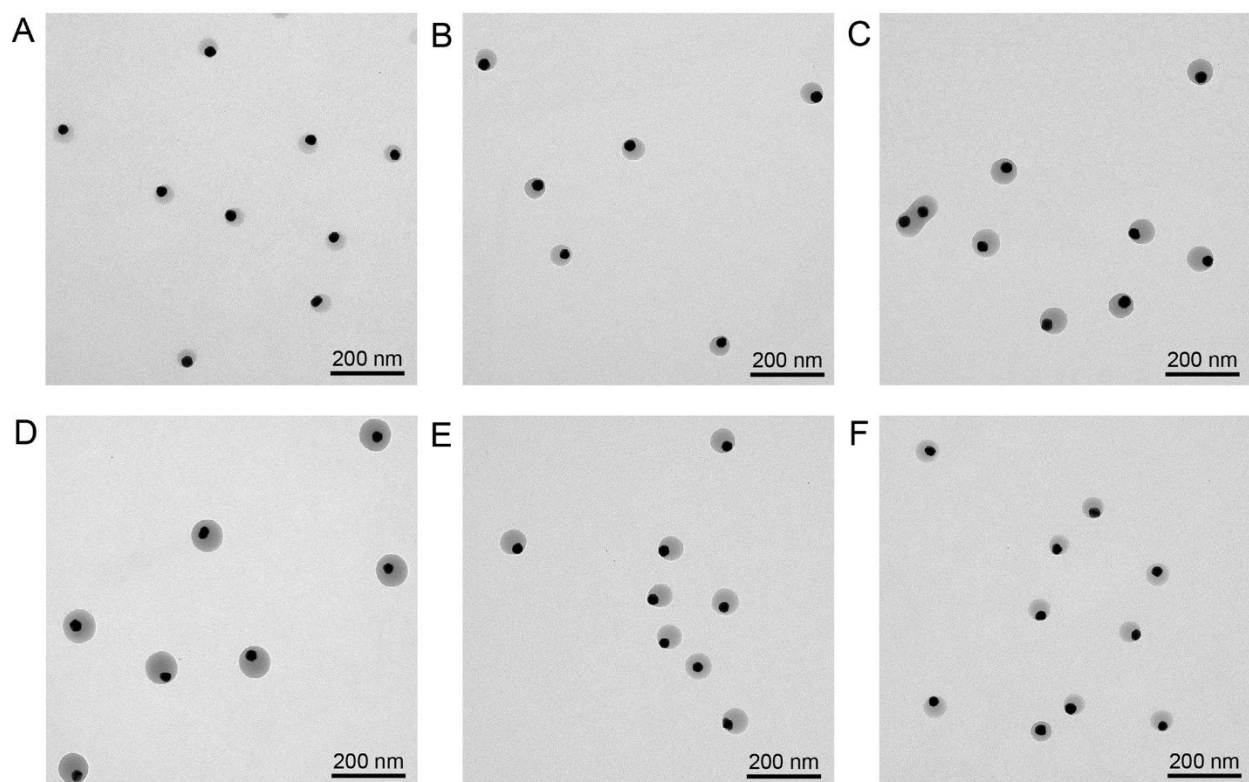


Fig. S32.

TEM images of Au-pBDT patchy nanoparticles prepared with 20 nm AuNPs with different reaction conditions. (A-D) Different concentration of BDT: 0.015 mg/mL (A), 0.03 mg/mL (B), 0.06 mg/mL (C), and 0.09 mg/mL (D), respectively. (E,F) Different concentration of AuNPs: 0.038 mg/mL (E), and 0.075 mg/mL (F). The results showed a similar trend with 60 nm AuNPs and therefore validate the BDT-mediated method as a robust strategy for Janus patchy nanoparticles.

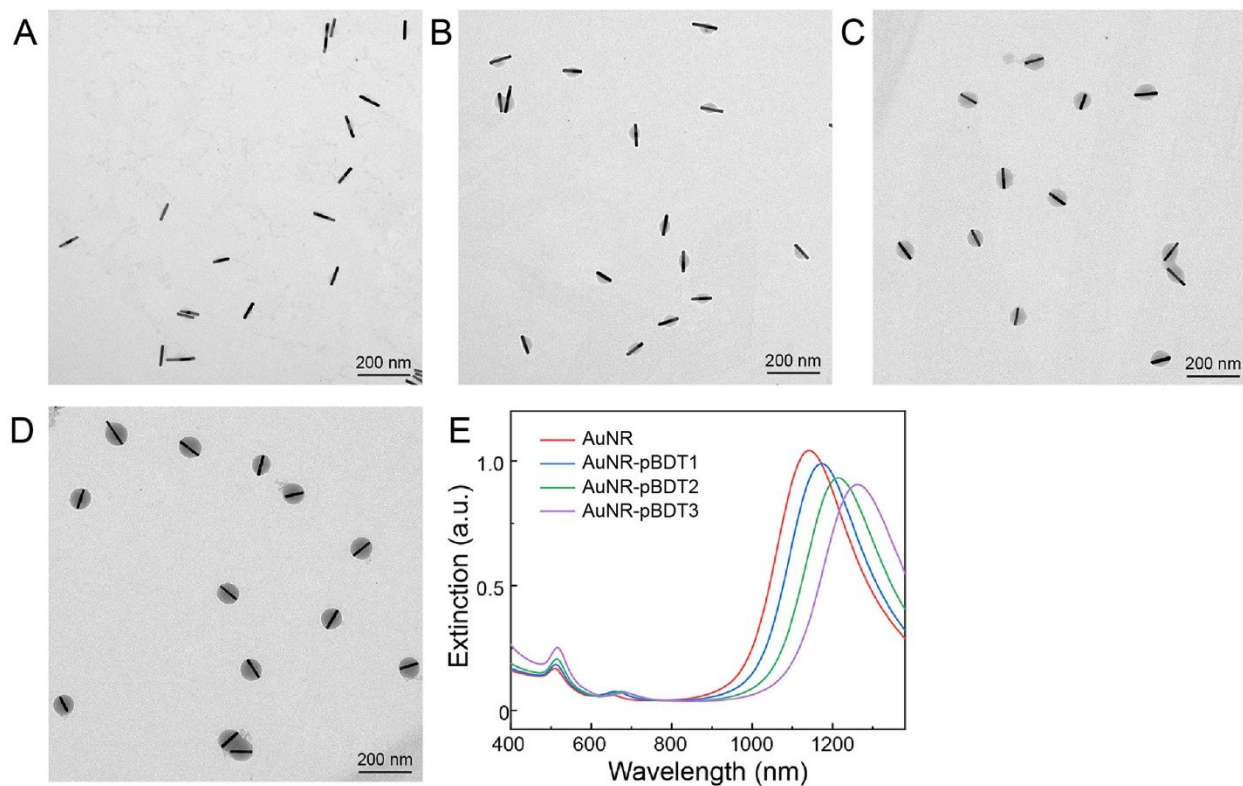


Fig. S33.

TEM images of AuNR-pBDT patchy nanoparticles prepared by using different amount of BDT. (A-D) Different concentration of BDT: 0.015 mg/mL (A), 0.03 mg/mL (B), 0.06 mg/mL (C), and 0.09 mg/mL (D), respectively. (E) UV-vis extinction spectra of the AuNR-pBDT. The results showed the good monodispersity of AuNR-pBDT. The red-shift of the LSPR peak suggested the successful pBDT coating and the potential use of pBDT to modulate the optical properties.

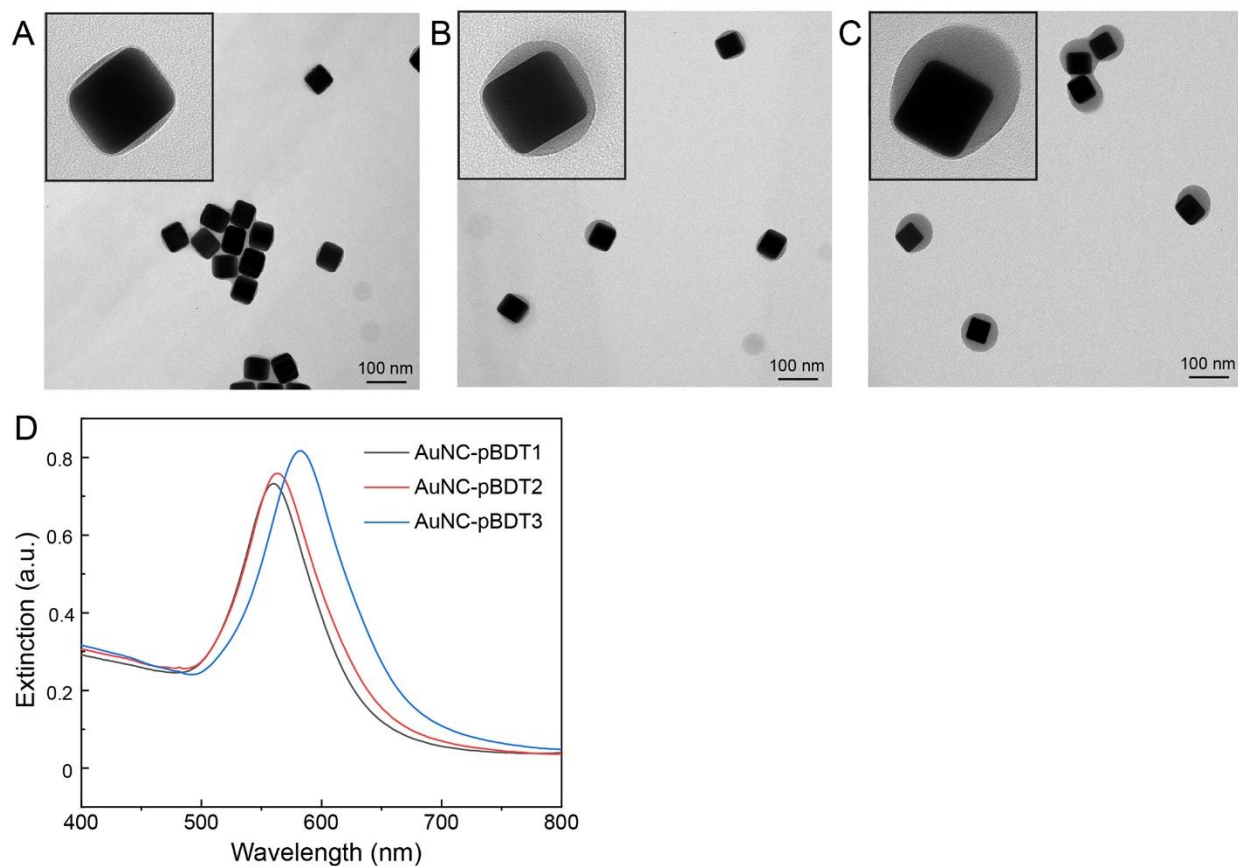


Fig. S34.

(A-C) TEM images of AuNC-pBDT patchy nanoparticles prepared by using different amount of BDT: 0.015 mg/mL (A), 0.03 mg/mL (B), and 0.06 mg/mL (C), respectively. (D) UV-vis extinction spectra of the AuNC-pBDT with different size of patches. The image results showed the good monodispersity of AuNC-pBDT. The red-shift of LSPR peak suggested successful pBDT coating.

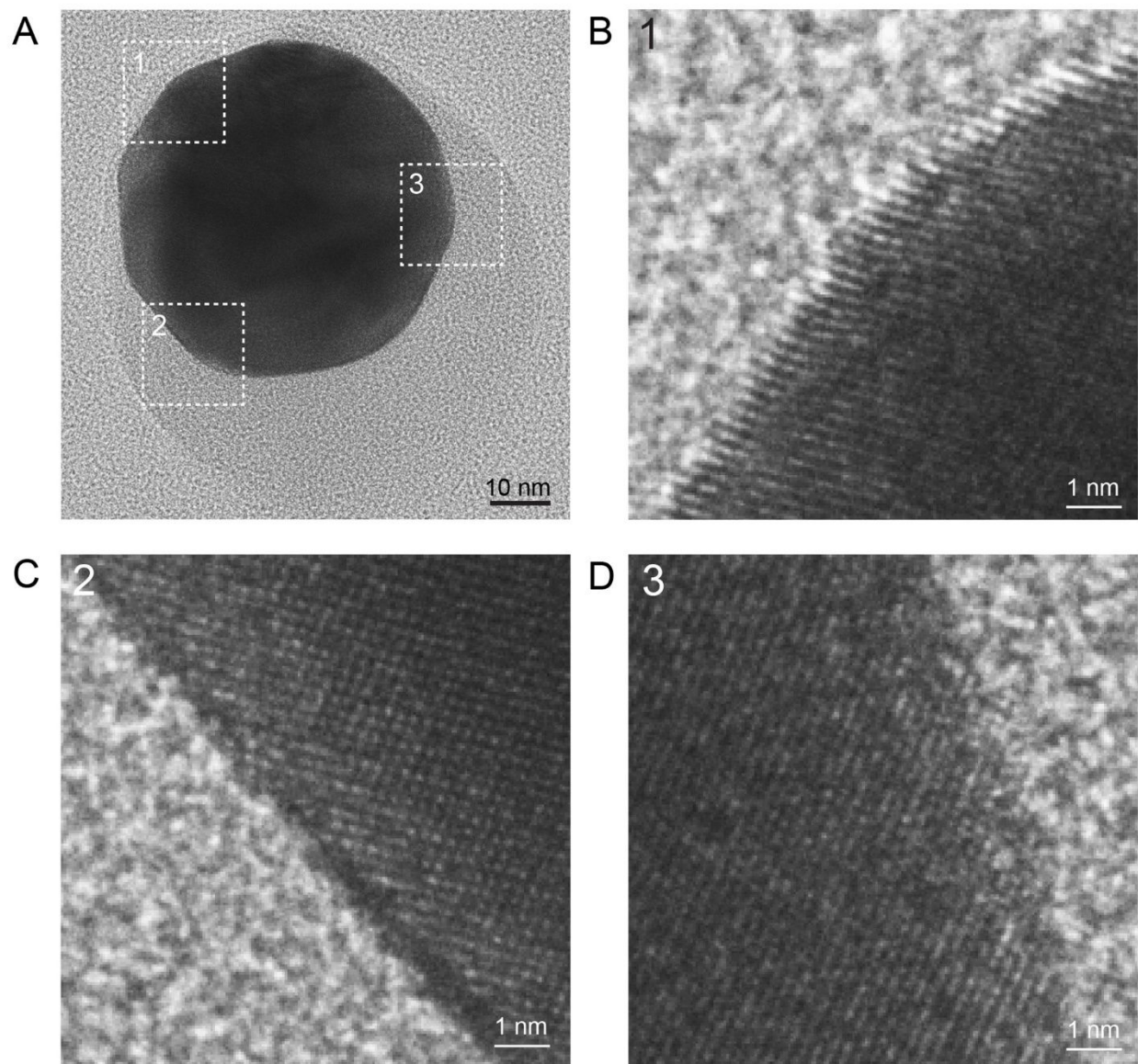


Fig. S35.

TEM images of an Au-pBDT patchy nanoparticle. (A) One representative Au-pBDT patchy Janus nanoparticle. The close-up image of the corresponding area (B, C, and D) as indicated in a. The irregular surface topography confirms the polycrystalline nature of the AuNPs used in this study.

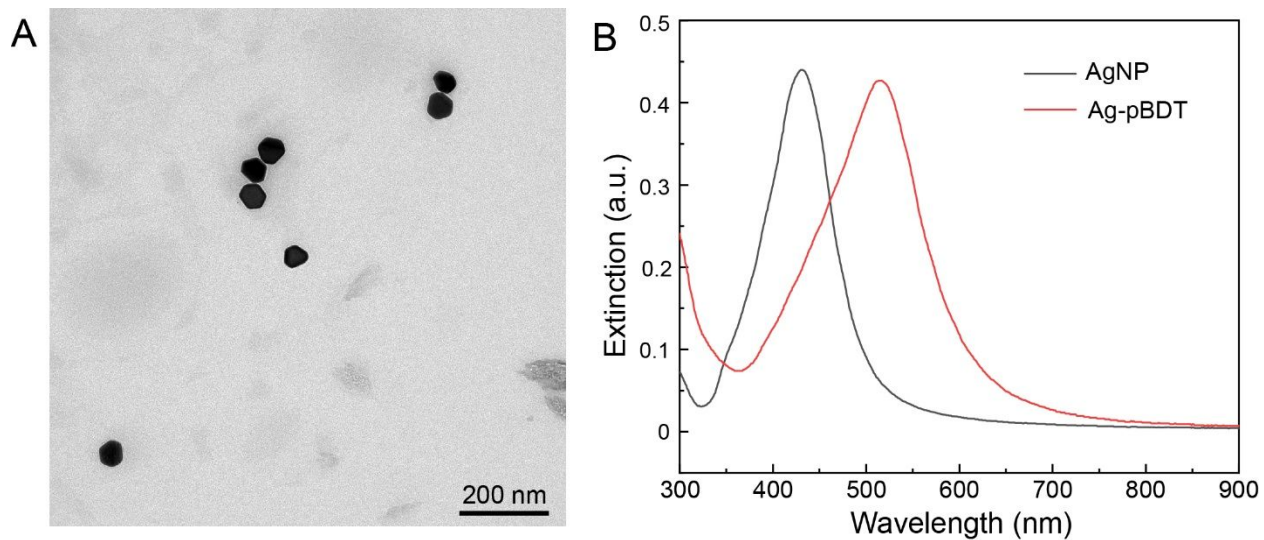


Fig. S36.

(A) TEM image of AgNPs. (B) UV-vis extinction spectra of the AgNPs and AgNP-pBDT patchy nanoparticles. The results showed the good monodispersity of AgNP-pBDT. The red-shift of LSPR peak suggested successful pBDT coating.

Table S1.

The experimental conditions employed for the synthesis of Au-pBDT patchy Janus nanoparticles.

Bicine buffer (pH 8.5, 10 mM) (mL)	AuNPs (OD=30) (μL)	SDS (0.5 wt%) (μL)	BDT (2 mg mL ⁻¹) (μL)	Overall size (nm)
Au concentration				
1.9	25	150	60	75 nm
1.9	50	150	60	72 nm
1.9	100	150	60	71 nm
1.9	150	150	60	68 nm
BDT concentration				
1.9	100	150	30	71 nm
1.9	100	150	60	79 nm
1.9	100	150	120	102 nm
1.9	100	150	240	140 nm
SDS concentration				
1.9	100	~0	80	156 nm
1.9	100	50	80	131 nm
1.9	100	100	80	115 nm
1.9	100	125	80	82 nm

Table S2.

Binding energy of different adsorbates to the gold slab. The results suggest that the BDT[-2q] and Fluo molecules have a strong affinity for the Au surface (gas phase binding energy of -2.74 eV/mol/molecule and -3.3 eV/mol/molecule, respectively).

Molecule	Fluorescein Sodium (Fluo)	(AAC)	BDT	BDT(-1q)	BDT(-2q)
Binding energy (eV)	-3.3	-1.54	-1.39	-2.42	-2.74

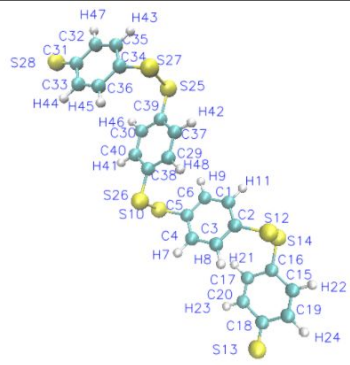
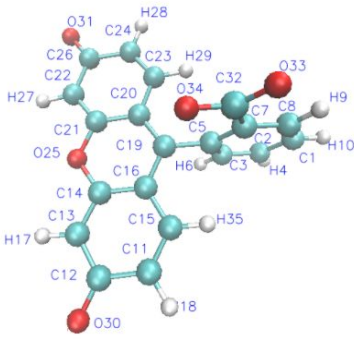
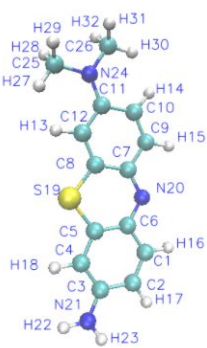
Table S3.

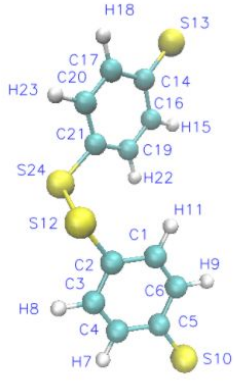
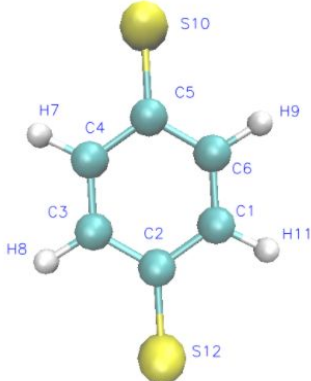
Comparison of BDT (-2q) binding energies to gold slab with low coverage and high coverage.

Molecule	BDT(-2q)
Binding energy/BDT Molecule High coverage	-2.12 eV
Binding energy/BDT Molecule Low Coverage	-2.74 eV

Table S4.

Atom-IDs and atom-charges of BDT/ pBDT₂/ pBDT₄/ Fluo/ AAC/ Au/ Na⁺/ Cl⁻/ water. BDT of different units were used to confirm the general assembly behavior in this study.

pBDT ₄ [-2q]			Fluo [-2q]			AAC [+1q]		
								
#ID	#type	charge	#ID	#type	charge	#ID	#type	charge
C1	C_R	-0.1467	C1	C_RA	-0.20743	C1	C_RC	-0.2311
C2	C_R	-0.24093	C2	C_RA	-0.21216	C2	C_RC	-0.21809
C3	C_R	-0.18138	C3	C_RA	-0.17247	C3	C_RC	0.44432
C4	C_R	-0.14271	H4	H_A	0.15835	C4	C_RC	-0.28245
C5	C_R	-0.2672	C5	C_RA	-0.20446	C5	C_RC	-0.18974
C6	C_R	-0.17959	H6	H_A	0.18326	C6	C_RC	0.21881
H7	H_	0.23303	C7	C_RA	-0.11122	C7	C_RC	0.23956
H8	H_	0.26612	C8	C_RA	-0.20138	C8	C_RC	-0.18418
H9	H_	0.25085	H9	H_A	0.19395	C9	C_RC	-0.22549
S10	S_3	0.04574	H10	H_A	0.15301	C10	C_RC	-0.24308
H11	H_	0.2319	C11	C_RA	-0.29722	C11	C_RC	0.40644
S12	S_3	-0.00146	C12	C_RA	0.26445	C12	C_RC	-0.32698
S13	S_3	-0.3592	C13	C_RA	-0.41172	H13	H_C	0.2536
S14	S_3	-0.0134	C14	C_RA	0.26746	H14	H_C	0.25871
C15	C_R	-0.08471	C15	C_RA	-0.20464	H15	H_C	0.25414
C16	C_R	-0.4177	C16	C_RA	-0.09905	H16	H_C	0.25527
C17	C_R	-0.10854	H17	H_A	0.16544	H17	H_C	0.25258
C18	C_R	-0.05769	H18	H_A	0.15275	H18	H_C	0.24634
C19	C_R	-0.30674	C19	C_RA	0.27451	S19	S_3C	0.46201
C20	C_R	-0.31558	C20	C_RA	-0.09834	N20	N_RC	-0.36904
H21	H_	0.21761	C21	C_RA	0.26753	N21	N_3C	-0.89784
H22	H_	0.19341	C22	C_RA	-0.41179	H22	H__AC	0.39836
H23	H_	0.19461	C23	C_RA	-0.20465	H23	H__AC	0.40174
H24	H_	0.19032	C24	C_RA	-0.29725	N24	N_3C	-0.41997
S25	S_3	-0.00134	O25	O_RA	-0.35781	C25	C_3C	-0.54913
S26	S_3	0.04578	C26	C_RA	0.2645	C26	C_3C	-0.54847
S27	S_3	-0.01333	H27	H_A	0.16543	H27	H_C	0.2623
S28	S_3	-0.35919	H28	H_A	0.15276	H28	H_C	0.26708
C29	C_R	-0.1797	H29	H_A	0.20086	H29	H_C	0.26708
C30	C_R	-0.18141	O30	O_2A	-0.474	H30	H_C	0.26444
C31	C_R	-0.05769	O31	O_2A	-0.47392	H31	H_C	0.26639

C32	C_R	-0.30672	C32	C_RA	0.32165	H32	H_C	0.26639									
C33	C_R	-0.31558	O33	O_2A	-0.496												
C34	C_R	-0.41767	O34	O_2A	-0.45121												
C35	C_R	-0.08472	H35	H_A	0.20081												
C36	C_R	-0.10865															
C37	C_R	-0.1469															
C38	C_R	-0.26721															
C39	C_R	-0.24095															
C40	C_R	-0.14254															
H41	H_	0.23304															
H42	H_	0.23188															
H43	H_	0.19341															
H44	H_	0.19459															
H45	H_	0.21754															
H46	H_	0.2663															
H47	H_	0.19034															
H48	H	0.25066															
pBDT₂ [-2q]			BDT [-2q]			Water											
						<table border="1"> <thead> <tr> <th>#ID</th><th>#type</th><th>charge</th></tr> </thead> <tbody> <tr> <td>H</td><td>HW</td><td>0.41700</td></tr> <tr> <td>O</td><td>OW</td><td>-0.83400</td></tr> </tbody> </table>			#ID	#type	charge	H	HW	0.41700	O	OW	-0.83400
#ID	#type	charge															
H	HW	0.41700															
O	OW	-0.83400															
						Cl⁻											
						<table border="1"> <thead> <tr> <th>#ID</th><th>#type</th><th>charge</th></tr> </thead> <tbody> <tr> <td>Cl⁻</td><td>CL</td><td>-1.00000</td></tr> </tbody> </table>			#ID	#type	charge	Cl ⁻	CL	-1.00000			
#ID	#type	charge															
Cl ⁻	CL	-1.00000															
						Na⁺											
						<table border="1"> <thead> <tr> <th>#ID</th><th>#type</th><th>charge</th></tr> </thead> <tbody> <tr> <td>Na⁺</td><td>NA</td><td>+1.00000</td></tr> </tbody> </table>			#ID	#type	charge	Na ⁺	NA	+1.00000			
#ID	#type	charge															
Na ⁺	NA	+1.00000															
						Au											
						<table border="1"> <thead> <tr> <th>#ID</th><th>#type</th><th>charge</th></tr> </thead> <tbody> <tr> <td>Au</td><td>AU</td><td>0.00000</td></tr> </tbody> </table>			#ID	#type	charge	Au	AU	0.00000			
#ID	#type	charge															
Au	AU	0.00000															
#ID	#type	charge	#ID	#type	charge												
C1	C_R	-0.18834	C1	C_R	-0.20301												
C2	C_R	-0.22669	C2	C_R	-0.12773												
C3	C_R	-0.1861	C3	C_R	-0.20301												
C4	C_R	-0.19149	C4	C_R	-0.20301												
C5	C_R	-0.14491	C5	C_R	-0.12773												
C6	C_R	-0.19385	C6	C_R	-0.20301												
H7	H_	0.17693	H7	H_	0.14107												
H8	H_	0.17569	H8	H_	0.14107												
H9	H_	0.18858	H9	H_	0.14107												
S10	S_3	-0.58379	S10	S_3	-0.74839												
H11	H_	0.20772	H11	H_	0.14107												
S12	S_3	-0.03375	S12	S_3	-0.74839												
S13	S_3	-0.58379															
C14	C_R	-0.14491															
H15	H_	0.18858															
C16	C_R	-0.19385															

C17	C_R	-0.19149		
H18	H_	0.17693		
C19	C_R	-0.18834		
C20	C_R	-0.1861		
C21	C_R	-0.22669		
H22	H_	0.20772		
H23	H_	0.17569		
S24	S_3	-0.03375		

Table S5.

The van der Waals /bond/angle/dihedral/improper parameters of BDT/ pBDT₂/ pBDT₄/ Fluo/ AAC/ Au/ Na⁺/ Cl⁻/ water.

BDT [-2q]	Pair_coeff	ϵ	σ								
		0.0951	3.47299041	#	C_R	C_R					
		0.0152	2.84642134	#	H_	H_					
		0.34400001	3.59032202	#	S_3	S_3					
	Bond	K_bond	r0								
				525	1.39	#	C_R	C_R			
350				1.02	#	C_R	H_				
350				1.73	#	S_3	C_R				
Angle	K_angle	θ_0									
	50	120	#	X	C_R	X					
Dihedral	K_dihedral	d	n								
	3.125	-1	2	#	X	C_R	C_R	X			
Improper	K_improper	ω_0									
	40	0	#	C_R	X	X	X				
pBDT₂ [-2q]	Pair_coeff	ϵ	σ								
		0.0951	3.47299041	#	C_R	C_R					
		0.0152	2.84642134	#	H_	H_					
		0.34400001	3.59032202	#	S_3	S_3					
	Bond	K_bond	r0								
				525	1.39	#	C_R	C_R			
				350	1.02	#	C_R	H_			
				350	1.73	#	S_3	C_R			
		350	2.07	#	S_3	S_3					
	Angle	K_angle	θ_0								
	50	92.1	#	X	S_3	X					
	50	120	#	X	C_R	X					
Dihedral	K_dihedral	d	n								
				3.125	-1	2	#	X	C_R	C_R	X
				0.5	-1	2	#	X	S_3	C_R	X
	1	1	2	#	X	S_3	S_3	X			
Improper	K_improper	ω_0									
	40	0	#	C_R	X	X	X				
pBDT₄ [-2q]	Pair_coeff	ϵ	σ								
		0.0951	3.47299041	#	C_R	C_R					
		0.0152	2.84642134	#	H_	H_					
		0.34400001	3.59032202	#	S_3	S_3					
	Bond	K_bond	r0								
				525	1.39	#	C_R	C_R			
350				1.02	#	C_R	H_				
350				1.73	#	S_3	C_R				
	350	2.07	#	S_3	S_3						
Angle	K_angle	θ_0									
	50	92.1	#	X	S_3	X					

		50	120	#	X	C_R	X	
	Dihedral	K_dihedral	d	n				
		3.125	-1	2	#	X	C_R C_R X	
		0.5	-1	2	#	X	S_3 C_R X	
		1	1	2	#	X	S_3 S_3 X	
	Improper	K_improper	ω_0					
		40		0	#	C_R X	X X	
Fluo [-2q]	Pair_coeff	ϵ	σ					
		0.0951	3.47299041	#	C_RA	C_RA		
		0.0152	2.84642134	#	H_A	H_A		
		0.0957	3.03315369	#	O_RA	O_RA		
		0.0957	3.03315369	#	O_2A	O_2A		
	Bond	K_bond	r0					
		525		1.39	#	C_RA	C_RA	
		350		1.02	#	C_RA	H_A	
		700		1.25	#	O_2A	C_RA	
		525		1.35	#	O_RA	C_RA	
	Angle	K_angle	θ_0					
		50		120	#	X	C_RA	X
		50		120	#	X	O_RA	X
	Dihedral	K_dihedral	d	n				
3.125		-1	2	#	X	C_RA C_RA X		
	6.25	-1	2	#	X	O_RA C_RA X		
Improper	K_improper	ω_0						
	40		0	#	C_RA X	X	X	
AAC [+1q]	Pair_coeff	ϵ	σ					
		0.0951	3.47299041	#	C_RC	C_RC		
		0.0152	2.84642134	#	H_C	H_C		
		0.34400001	3.59032202	#	S_3C	S_3C		
		0.0774	3.26256026	#	N_RC	N_RC		
		0.0774	3.26256026	#	N_3C	N_3C		
		0	2.84642134	#	H__AC	H__AC		
		0.0951	3.47299041	#	C_3C	C_3C		
	Bond	K_bond	r0					
		350		1.09	#	C_3C	H_C	
		525		1.39	#	C_RC	C_RC	
		350		1.02	#	C_RC	H_C	
		350		1.462	#	N_3C	C_3C	
		350		1.392	#	N_3C	C_RC	
350			1.022	#	N_3C	H__AC		
525			1.34	#	N_RC	C_RC		
	350		1.73	#	S_3C	C_RC		
Angle	K_angle	θ_0						
	50		109.471	#	X	C_3C	X	
	50		120	#	X	C_RC	X	
	50		106.7	#	X	N_3C	X	

		50	120 #	X	N_RC	X
		50	92.1 #	X	S_3C	X
	Dihedral	K_dihedral	d n			
		3.125	-1 2 #	X	C_RC	C_RC X
		0.166667	1 3 #	X	N_3C	C_3C X
		0.25	1 3 #	X	N_3C	C_RC X
		6.25	-1 2 #	X	N_RC	C_RC X
		0.5	-1 2 #	X	S_3C	C_RC X
	Improper	K_improper	ω_0			
		40	0 #	C_RC X	X	X
Au	Pair_coeff	ϵ	σ			
		5.29	2.62904212 #	AU	AU	
Na⁺	Pair_coeff	ϵ	σ			
		0.0874	2.43928069 #	Na+	Na+	
Cl⁻	Pair_coeff	ϵ	σ			
		0.0356	4.47765696 #	Cl-	Cl-	
water	Pair_coeff	ϵ	σ			
		0.1521	3.15069895 #	OW	OW	
		0	0 #	HW	HW	
	Bond	K_bond	r0			
		4500	0.9572 #	HW	OW	
	Angle	K_angle	θ_0			
		550	104.52 #	HW	OW	HW
<p>The units of energy, distance, and angle are kcal/mol, Angstrom and degree, respectively. Lennard-Jones equation is $E = 4\epsilon[(\sigma/r)^{12} - (\sigma/r)^6]$. Harmonic equations are $E = K_{bond}(r-r_0)^2$ (for bond), $E = K_{angle}(\theta - \theta_0)^2$ (for angle) and $E = K_{dihedral}(1 + d\cos(n\phi))$ (for dihedral). Umbrella equations are $E = 0.5K_{improper}(1/\sin\omega_0)^2(\cos\omega - \cos\omega_0)^2$ and $E = K_{improper}(1 - \cos\omega)$ for $\omega_0 \neq 0^\circ$ and $\omega_0 = 0^\circ$ cases, respectively. It is noted that the bonds and angles of water molecules are fixed with the fix shake command.</p>						

Table S6.

The solvation free energies of BDT/ pBDT₂/pBDT₄/Fluo/AAC in water solvent at 298 K, 1atm. Our molecular dynamics (MD) results show that these binding energies are strongly modulated by the relative solvation energies. In fact, our MD simulations indicate that even though the BDT[-2q] and Fluo molecules demonstrated much stronger affinity to the Au surface compared to AAC, the AAC molecules quickly attached on Au substrate for an enhanced interfacial population due to its relatively low solubility (we calculate the AAC solvation free energy of -87.69 kcal/mol/molecule, compared to -119.43 kcal/mol/molecule and -230.75 kcal/mol/molecule for Fluo and BDT, respectively).

Type of solute	Number of solute molecules	Number of solvent molecules	FEP [kcal/mol]
BDT [-2q]	1	333	-230.750
pBDT ₂ [-2q]	1	666	-179.250
pBDT ₄ [-2q]	1	1665	-146.768
Fluo [-2q]	1	666	-119.425
AAC [+1q]	1	666	-87.6873

Movie S1.

3D electron tomography reconstruction of Janus patchy nanoparticles.

Movie S2.

3D electron tomography reconstruction of tetrahedral patchy nanoparticles.